

Generalized Two-Dimensional Quaternion Principal Component Analysis with Weighting for Color Image Recognition

Zhi-Gang Jia, Zi-Jin Qiu, Qian-Yu Wang, Mei-Xiang Zhao and Dan-Dan Zhu

Abstract—One of the most powerful methods of color image recognition is the two-dimensional principle component analysis (2DQPCA) approach, which is based on quaternion representation and preserves color information very well. However, the current versions of 2DQPCA are still not feasible to extract different geometric properties of color images according to practical data analysis requirements and they are vulnerable to strong noise. In this paper, a generalized 2DQPCA approach with weighting is presented with imposing L_p norms on both constraint and objective functions. As a unit 2DQPCA framework, this new version makes it possible to choose adaptive regularizations and constraints according to actual applications and can extract both geometric properties and color information of color images. The projection vectors generated by the deflating scheme are required to be orthogonal to each other. A weighting matrix is defined to magnify the effect of main features. This overcomes the shortcomings of traditional 2DQPCA that the recognition rate decreases as the number of principal components increases. The numerical results based on the real face databases validate that the newly proposed method is robust to noise and performs better than the state-of-the-art 2DQPCA-based algorithms and four prominent deep learning methods.

Index Terms—Generalized 2DQPCA; Weighted projection; Color face recognition; Color image reconstruction; Neural networks.

1 INTRODUCTION

Color image recognition becomes more and more important in recent data science. Two dimensional quaternion principle analysis was proposed to scratch the features of color face images [1] and had been well developed for the dimensional reduction and the color image reconstruction [2]–[5]. This contributes to the development of the fundamental tool—the principal component analysis—of machine learning frameworks. The two dimensional quaternion principle analysis based approaches have the advantages at preserving the spatial structure and color information of color images and costing less computational operations. However, the geometric properties (such as sparsity) of color images are not well extracted and the current versions of two dimensional quaternion principle analysis are still not robust to treat color images polluted by noise. In this paper, we present a generalized two dimensional quaternion principle analysis with utilizing L_p -norms of quaternion vectors to obtain more geometrical and color information

and to resist more kinds of noises. Our aim is to present a new approach for color image recognition, which significantly promotes the robustness and the recognition rate.

It is well known that two dimensional quaternion principle analysis (2DQPCA) generalizes two dimensional principle analysis (2DPCA) [6] to the quaternion skew-field with a strong motivation of applying the color information of color images. Recall that principal component analysis (PCA) [7] is an unsupervised learning approach for feature extraction and dimension reduction. It has been widely used in the fields of computer vision and pattern recognition. Recently, many robust PCA (RPCA) algorithms are proposed with improving the quadratic formulation, which renders PCA vulnerable to noises, into L_1 -norm on the objection function, e.g., L_1 -PCA [8], R_1 -PCA [9], and PCA- L_1 [10]. Besides of robustness, sparsity is also a desired property. By applying L_0 -norm or L_1 -norm on the constraint function (also called penalty or regularization [11], [12]) of PCA, a series of sparse PCA (SPCA) algorithms have been proposed in [13]–[17]. In order to enhance both robustness and sparsity at the same time, robust sparse PCA (RSPCA) is further developed, see [18] and [19] for instance. Considering that L_0 -norm, L_1 -norm and L_2 -norm are all special cases of L_p -norm, it is natural to replace the L_2 -norm in traditional PCA with arbitrary norm, both on its objective function and constraint function, as proposed in generalized PCA (GPCA) [20], [21].

When being applied to extract feature from images, PCA treats each sample as a vector, and hence, 2D images are converted to high-dimensional vectors prior to feature extraction [7]. To avoid the intensive computation of high-dimensional data, Yang *et al.* [6] proposed the 2DPCA approach, which constructs the covariance matrix by directly using 2D face image matrices. 2DPCA directly constructs

The work of the authors is partially supported by National Natural Science Foundation of China under grants 12171210, 12090011 and 11771188; the Natural Science Foundation of the Jiangsu Higher Education Institutions of China under grant 21KJA110001; the Priority Academic Program Development Project (PAPD); the Top-notch Academic Programs Project (No. PPZY2015A013) of Jiangsu Higher Education Institutions.

- Z.-G. Jia is with the School of Mathematics and Statistics, Jiangsu Normal University, Xuzhou 221116, China; and with the Research Institute of Mathematical Science, Jiangsu Normal University, Xuzhou 221116, China.
E-mail: zhgjia@jsnu.edu.cn
- Z.-J. Qiu, Q.-Y. Wang and D.-D. Zhu are with the School of Mathematics and Statistics, Jiangsu Normal University, Xuzhou 221116, China.
- M.-X. Zhao is with School of Information and Control Engineering, China University of Mining and Technology, Xuzhou 221116, China; and with the School of Mathematics and Statistics, Jiangsu Normal University, Xuzhou 221116, China.

the sample covariance matrix from the two-dimensional image, which reduces the burden of calculating the sample covariance matrix from the high-dimensional vectors, and therefore has higher computational efficiency. In addition, 2DPCA processes a two-dimensional matrix to preserve the spatial structure of the images [6], [22], [23], and achieves a higher face recognition rate than PCA in most cases. This image-as-matrix method offers insights for improving above RSPCA, PCA- L_p , GPCA, etc. The L_1 -norm based 2DPCA (2DPCA- L_1) [24] and 2DPCA- L_1 with sparsity (2DPCA- L_1S) [25] are two typical improvements of PCA- L_1 and RSPCA, respectively. And the generalized 2DPCA (G2DPCA) [26] imposes L_p -norm on both objective and constraint functions of 2DPCA. Recently, Chen *et al.* [27] further proposed the R2DPCA algorithm, which utilizes the label information (if known) of training samples to calculate a relaxation vector and presents a weight to each subset of training data.

To process color images, the above method separately processes three color channels or connects the representations of different color channels into a large matrix, so cross-channel correlation is not considered [28], [29]. However, this correlation is very important for color image processing. Xiang *et al.* [30] proposed a CPCA approach for color face recognition. They utilized a color image matrix representation model based on the framework of PCA and applied 2DPCA to compute the optimal projection for feature extraction. Zou *et al.* [31] then presented quaternion collaborative representation-based classification (QCRC) and quaternion sparse RC (QSRC) using quaternion L_1 minimization. For color face recognition, a series of quaternion-based methods, such as the quaternion PCA (QPCA) [32], the two-dimensional QPCA (2DQPCA), the bidirectional 2DQPCA [33], the kernel QPCA (KQPCA) and the two-dimensional KQPCA [34], have been proposed, with generalizing the conventional PCA and 2DPCA. Recently, Jia *et al.* [1] presented the 2DQPCA approach based on quaternion models with reducing the feature dimension in row direction. Xiao and Zhou [3] proposed novel quaternion ridge regression models for 2DQPCA with reducing the feature dimension in column direction and two-dimensional quaternion sparse principle component analysis. Zhao *et al.* [2] further improved the 2DQPCA into abstracting the features of quaternion matrix samples in both row and column directions. Lately, Xiao *et al.* [4] proposed a two-dimensional quaternion sparse discriminant analysis (2D-QSDA), including sparse regularization, that meets the requirements of representing RGB and RGB-D images. These 2DQPCA-like approaches can preserve the spatial structure of color images and have a low computation cost. They have achieved a significant success in promoting the robustness and the ratio of face recognition by utilizing color information.

In addition to PCA-like methods, LDA and its variants are still one kind of feature extraction algorithms which play an important role in pattern recognition and computer vision; see [35]–[37] for instance. Besides of color face recognition, many recent studies (e.g. [38]–[41]) also have shown that the quaternion framework is well adapted to color image restoration by encoding the color channels into the three imaginary parts.

Nowadays, the color face recognition problem faces

more complicated backgrounds, noise interference, and higher recognition accuracy requirements. There is still a lack of mathematical models that can reflect physical properties, are more interpretable, and are better than neural network methods. Thus, we took a small step towards this goal, established a general mathematical model and established a comprehensive and systematic solution method. The contribution of this paper is listed in three aspects.

- A novel generalized two-dimensional quaternion principal component analysis (G2DQPCA) is presented as a general framework that offers the great flexibility to fit various real-world applications. To utilize the first-order condition of convex quaternion function, a new definition is proposed for the derivative of the quaternion norm. A closed-form solution is obtained at each step of iteration.
- A new weighted G2DQPCA (WG2DQPCA) approach is proposed for color face recognition. The projection bases are mathematically required to be orthogonal to each other and are weighted by corresponding objective function value to enhance the role of main features in color image recognition.
- Based on three standard color face databases, the evaluation of proposed methods is implemented on color face recognition and color image reconstruction. Numerical results indicate that WG2DQPCA performs better than the state-of-the-art 2DQPCA-based algorithms and four prominent deep learning methods.

The paper is organized as follows. In Section 2, the fundamental information of quaternion matrix theory is recalled. In Section 3, a generalized two-dimensional color principal component analysis with weighted projection approach is presented based on quaternion models and a closed-form solution is derived. In Section 4, the WG2DQPCA and G2DQPCA approaches are proposed for face recognition and image reconstruction, respectively. In Section 5, numerical experiments are conducted by applying the Georgia Tech face database, Color FERET face database and the Faces95 database. Finally, the conclusion is given in Section 6.

2 PRELIMINARIES

In this section, we recall the basic information of quaternions, quaternion vectors and quaternion matrices.

Let us firstly describe some notation. Letters of regular font denote scalars, vectors and matrices in the real domain. Boldface letters denote quaternions, quaternion vectors and quaternion matrices. $\text{sign}(\cdot)$ denotes the sign function; $|\cdot|$ denotes the absolute value; $w \circ v$ denotes the Hadamard product, i.e., the element-wise product between two vectors; $\|\cdot\|_1$, $\|\cdot\|_2$, and $\|\cdot\|_p$ denote L_1 -norm, L_2 -norm, and L_p -norm, respectively.

Let \mathbf{i} , \mathbf{j} , \mathbf{k} be three imaginary units satisfying

$$\mathbf{i}^2 = \mathbf{j}^2 = \mathbf{k}^2 = \mathbf{ijk} = -1$$

and let

$$\mathbb{Q} = \left\{ \mathbf{a} = a^{(0)} + a^{(1)}\mathbf{i} + a^{(2)}\mathbf{j} + a^{(3)}\mathbf{k} \mid a^{(0)}, \dots, a^{(3)} \in \mathbb{R} \right\}$$

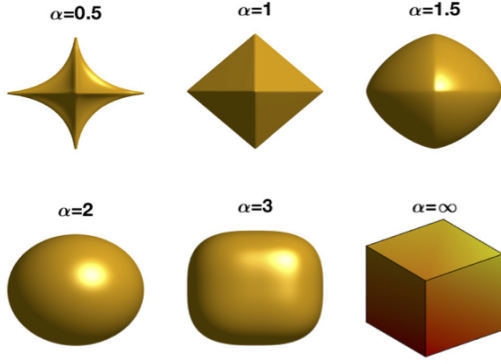


Fig. 1: Purely imaginary quaternions with s -absolute values equal to or less than 1 ($|\mathbf{a}|_\alpha \leq 1$).

denote the quaternion skew-field.

DEFINITION 2.1. For a quaternion $\mathbf{a} \in \mathbb{Q}$ and a positive real number $\alpha \in \mathbb{R}$, the s -absolute value of \mathbf{a} is defined by

$$|\mathbf{a}|_\alpha \equiv \sqrt[\alpha]{|a^{(0)}|^\alpha + |a^{(1)}|^\alpha + |a^{(2)}|^\alpha + |a^{(3)}|^\alpha}.$$

For illustration, we plot the set of purely quaternion numbers satisfying $|\mathbf{a}|_\alpha \leq 1$ in Figure 1. If $\alpha = 2$, then $|\mathbf{a}|_\alpha$ is exactly the absolute of \mathbf{a} , shortly denoted by $|\mathbf{a}|$. The sign of a quaternion \mathbf{a} is defined by

$$\text{sign}(\mathbf{a}) \equiv \begin{cases} \mathbf{a}/|\mathbf{a}|, & \text{if } \mathbf{a} \neq 0, \\ 0, & \text{if } \mathbf{a} = 0. \end{cases}$$

An $m \times n$ quaternion matrix is of the form $\mathbf{A} = A^{(0)} + A^{(1)}\mathbf{i} + A^{(2)}\mathbf{j} + A^{(3)}\mathbf{k}$, where $A^{(0)}, \dots, A^{(3)} \in \mathbb{R}^{m \times n}$. A quaternion is a *pure quaternion* if its real part is zero. A *pure quaternion matrix* is a matrix whose elements are pure quaternions ($A^{(0)} = 0$) or zero. In the RGB color space, a pixel can be represented with a pure quaternion, $r\mathbf{i} + g\mathbf{j} + b\mathbf{k}$, where r, g, b stand for the values of Red, Green and Blue components, respectively. An $m \times n$ color image can be saved as an $m \times n$ pure quaternion matrix, $\mathbf{A} = [\mathbf{a}_{ij}]_{m \times n}$, in which each entry, $\mathbf{a}_{ij} = r_{ij}\mathbf{i} + g_{ij}\mathbf{j} + b_{ij}\mathbf{k}$, denotes one color pixel, and r_{ij}, g_{ij} and b_{ij} are nonnegative integers [40], [43].

2.1 Norms of quaternion vectors

An n -dimensional quaternion vector is of the form

$$\mathbf{w} = [\mathbf{w}_i]_n = w^{(0)} + w^{(1)}\mathbf{i} + w^{(2)}\mathbf{j} + w^{(3)}\mathbf{k},$$

where $\mathbf{w}_i \in \mathbb{Q}$ denotes the i -th entry of \mathbf{w} , and $w^{(0)}, \dots, w^{(3)} \in \mathbb{R}^n$. The sign and the absolute value of a quaternion vector are defined in the element-wise manner, that is

$$|\mathbf{w}| \equiv [|\mathbf{w}_i|]_n, \quad (2.1a)$$

$$\text{sign}(\mathbf{w}) \equiv [\text{sign}(\mathbf{w}_i)]_n. \quad (2.1b)$$

DEFINITION 2.2. Let α and p be two positive real numbers, the $L_{\alpha,p}$ -norm of a quaternion vector $\mathbf{w} \in \mathbb{Q}^n$ is defined by

$$\|\mathbf{w}\|_{\alpha,p} \equiv \left(\sum_{i=1}^n |\mathbf{w}_i|_\alpha^p \right)^{\frac{1}{p}}.$$

If $\alpha = p = 2$, the $L_{\alpha,p}$ -norm reduces to the L_2 -norm. Because the α -absolute value quaternions have different

geometric properties, people expect to apply different $L_{\alpha,p}$ -norms in the regularization constrains to obtain especial features of color images. In the following text, we set α as the default value 2 to clarify the reasonability of the theory, and drop α from the subscript for simplicity. That means the L_p -norm of quaternion vector \mathbf{w} is denoted by

$$\|\mathbf{w}\|_p = \left(\sum_{i=1}^n |\mathbf{w}_i|^p \right)^{\frac{1}{p}}. \quad (2.2)$$

2.2 The real structure-preserving method

Since the computation of quaternion matrices usually costs a lot of CPU times, we always apply the structure-preserving method (see [44], [45], etc.) to simulate the calculation of quaternions only by real operations.

For quaternion matrix $\mathbf{A} = A^{(0)} + A^{(1)}\mathbf{i} + A^{(2)}\mathbf{j} + A^{(3)}\mathbf{k} \in \mathbb{Q}^{m \times n}$ and quaternion vector $\mathbf{w} = w^{(0)} + w^{(1)}\mathbf{i} + w^{(2)}\mathbf{j} + w^{(3)}\mathbf{k} \in \mathbb{Q}^n$, we define their real representations by

$$\mathbf{A}^{(\Upsilon)} \equiv \begin{bmatrix} A^{(0)} & -A^{(1)} & -A^{(2)} & -A^{(3)} \\ A^{(1)} & A^{(0)} & -A^{(3)} & A^{(2)} \\ A^{(2)} & A^{(3)} & A^{(0)} & -A^{(1)} \\ A^{(3)} & -A^{(2)} & A^{(1)} & A^{(0)} \end{bmatrix} \quad (2.3)$$

and

$$\mathbf{w}^{(\gamma)} \equiv [(w^{(0)})^T \ (w^{(1)})^T \ (w^{(2)})^T \ (w^{(3)})^T]^T, \quad (2.4)$$

respectively. Note that $\mathbf{w}^{(\gamma)}$ is a $4n$ -dimensional real vector. For convenience, the absolute value, sign and $L_{2,p}$ -norm of $\mathbf{w}^{(\gamma)}$ are defined by

$$|\mathbf{w}^{(\gamma)}|_Q \equiv (|\mathbf{w}| + |\mathbf{w}\mathbf{i}| + |\mathbf{w}\mathbf{j}| + |\mathbf{w}\mathbf{k}|)^{(\gamma)}, \quad (2.5a)$$

$$\text{sign}_Q(\mathbf{w}^{(\gamma)}) \equiv (\text{sign}(\mathbf{w}))^{(\gamma)}, \quad (2.5b)$$

$$\|\mathbf{w}^{(\gamma)}\|_{2,p} \equiv \left[\sum_{i=1}^n \left(\sqrt{\sum_{k=0}^3 (\mathbf{w}_{kn+i}^{(\gamma)})^2} \right)^p \right]^{\frac{1}{p}}. \quad (2.5c)$$

It's easy to verify that $\|\mathbf{w}^{(\gamma)}\|_{2,p}$ is a vector norm on the real vector space if $p \geq 1$. If $0 < p < 1$, $\|\mathbf{w}^{(\gamma)}\|_{2,p}$ is regarded as a non-convex and non-Lipschitz continuous function. The L_p -norm of quaternion vector \mathbf{w} can be equivalently written as

$$\|\mathbf{w}\|_p^p = \sum_{i=1}^n |\mathbf{w}_i|^p = \sum_{i=1}^n \left(\sqrt{\sum_{j=0}^3 (w_i^{(j)})^2} \right)^p = \|\mathbf{w}^{(\gamma)}\|_{2,p}^p.$$

The definitions in (2.5) make it convenient to convert between quaternion vector norm and real vector norm equivalently.

3 GENERALIZED 2DQPCA

In this section, we present a new generalized 2DQPCA (G2DQPCA) and quaternion optimization algorithms.

3.1 G2DQPCA

Suppose that $\mathbf{F}_1, \mathbf{F}_2, \dots, \mathbf{F}_\ell \in \mathbb{Q}^{m \times n}$ are ℓ training samples of the quaternion matrix form and their mean is

$$\Psi = \frac{1}{\ell} \sum_{i=1}^{\ell} \mathbf{F}_i \in \mathbb{Q}^{m \times n}.$$

In the new G2DQPCA, the features are extracted by solving a quaternion optimization model with L_s -norm in the objective function and L_p -norm in constraints:

$$\begin{aligned} (\widehat{\mathbf{w}}_1, \dots, \widehat{\mathbf{w}}_k) &= \arg \max_{\mathbf{w}_1, \dots, \mathbf{w}_k \in \mathbb{Q}^n} \sum_{j=1}^k \sum_{i=1}^{\ell} \|(\mathbf{F}_i - \Psi) \mathbf{w}_j\|_s^s, \\ \text{s.t. } \|\mathbf{w}_j\|_p^p &= 1, \mathbf{w}_j^* \mathbf{w}_i = 0, i \neq j, i, j = 1, \dots, k, \end{aligned} \quad (3.1)$$

where $s \geq 1, p > 0$. The constraint $\|\mathbf{w}_j\|_p^p = 1$ is convex if $p \geq 1$ and non-convex if $0 < p < 1$. The constraint set is either convex or non-convex depending on the value of p .

Now we are concerned with the solvability of the optimization problem (3.1). As primary results, several necessary inequalities are derived for a linear optimization problem with L_p -norm in quaternion domain. Their proofs are based on the first-order condition of convex function [11]. Let $w, v \in \mathbb{R}^n$ be two real vectors and let $f(w)$ be a convex and differentiable a real function. Then

$$f(w) \geq f(v) + \nabla f(v)^T (w - v), \quad (3.2)$$

where ∇ denotes the gradient operator, and the equality holds when $w = v$.

THEOREM 3.1. *Let $\mathbf{w}, \mathbf{v} \in \mathbb{Q}^n$ be two quaternion vectors and $p \geq 1$, then there is*

$$\|\mathbf{w}\|_p^p \geq p \left[|\mathbf{v}^{(\gamma)}|_Q^{p-1} \circ \text{signQ}(\mathbf{v}^{(\gamma)}) \right]^T \mathbf{w}^{(\gamma)} + (1-p) \|\mathbf{v}\|_p^p \quad (3.3)$$

and the equality holds when $\mathbf{w} = \mathbf{v}$.

Proof. Denote $\mathbf{w} = [\mathbf{w}_1, \dots, \mathbf{w}_n]^T$, $\mathbf{v} = [\mathbf{v}_1, \dots, \mathbf{v}_n]^T$, $\mathbf{w}_i, \mathbf{v}_i \in \mathbb{Q}$. By the real structure-preserving method, we only need to prove

$$\|\mathbf{w}^{(\gamma)}\|_{2,p}^p \geq p \left[|\mathbf{v}^{(\gamma)}|_Q^{p-1} \circ \text{signQ}(\mathbf{v}^{(\gamma)}) \right]^T \mathbf{w}^{(\gamma)} + (1-p) \|\mathbf{v}^{(\gamma)}\|_{2,p}^p.$$

Firstly, we assume all entries of \mathbf{v} are non-zero elements. Then $\|\mathbf{w}^{(\gamma)}\|_{2,p}^p$ is differentiable at $\mathbf{w}^{(\gamma)} = \mathbf{v}^{(\gamma)}$, and

$$\frac{\partial \|\mathbf{w}^{(\gamma)}\|_{2,p}^p}{\partial \mathbf{w}^{(\gamma)}} = [y_0^T \ y_1^T \ y_2^T \ y_3^T]^T,$$

where for $j = 0, 1, 2, 3$,

$$y_j = \left[p \frac{|\mathbf{w}_1|^{p-1}}{|\mathbf{w}_1|} w_1^{(j)} \quad p \frac{|\mathbf{w}_2|^{p-1}}{|\mathbf{w}_2|} w_2^{(j)} \quad \dots \quad p \frac{|\mathbf{w}_n|^{p-1}}{|\mathbf{w}_n|} w_n^{(j)} \right]^T.$$

Applying the definitions in (2.5), we obtain

$$\begin{aligned} \nabla \|\mathbf{w}^{(\gamma)}\|_{2,p}^p &\equiv \frac{\partial \|\mathbf{w}^{(\gamma)}\|_{2,p}^p}{\partial \mathbf{w}^{(\gamma)}} \Big|_{\mathbf{w}=\mathbf{v}} \\ &= p \cdot |\mathbf{v}^{(\gamma)}|_Q^{p-1} \circ \text{signQ}(\mathbf{v}^{(\gamma)}). \end{aligned} \quad (3.4)$$

Clearly,

$$|\mathbf{v}^{(\gamma)}|_Q^{p-1} \circ \text{signQ}(\mathbf{v}^{(\gamma)})^T \mathbf{v}^{(\gamma)} = \|\mathbf{v}^{(\gamma)}\|_{2,p}^p. \quad (3.5)$$

Additionally, $\|\mathbf{w}^{(\gamma)}\|_{2,p}^p$ is a convex function because $p \geq 1$. Together with equality (3.4), applying the first-order convexity condition (3.2) to the function $f(\cdot) = \|\cdot\|_{2,p}^p$ yields the desired result

$$\begin{aligned} &\|\mathbf{w}^{(\gamma)}\|_{2,p}^p \\ &\geq \|\mathbf{v}^{(\gamma)}\|_{2,p}^p + (\nabla \|\mathbf{v}^{(\gamma)}\|_{2,p}^p)^T (\mathbf{w}^{(\gamma)} - \mathbf{v}^{(\gamma)}) \\ &= p \left[|\mathbf{v}^{(\gamma)}|_Q^{p-1} \circ \text{signQ}(\mathbf{v}^{(\gamma)}) \right]^T \mathbf{w}^{(\gamma)} \\ &\quad + (1-p) \|\mathbf{v}^{(\gamma)}\|_{2,p}^p \end{aligned} \quad (3.6)$$

where the equality holds when $\mathbf{w} = \mathbf{v}$.

Now we consider the case that \mathbf{v} has zero entries. For any two quaternions \mathbf{w}_i and \mathbf{v}_i , there is

$$\begin{aligned} |\mathbf{w}_i|^p &\geq p \cdot |\mathbf{v}_i|^{p-1} \cdot (\text{signQ}(\mathbf{v}_i^{(\gamma)}))^T \mathbf{w}_i^{(\gamma)} \\ &\quad + (1-p) |\mathbf{v}_i|^p. \end{aligned} \quad (3.7)$$

If $\mathbf{v}_i \neq 0$, this inequality is exactly (3.6) being applied to two quaternions, because $|\mathbf{w}_i|^p = \left(\sqrt{\sum_{j=0}^3 (w_i^{(j)})^2} \right)^p$ is convex and differentiable at $\mathbf{w}_i = \mathbf{v}_i$. If $\mathbf{v}_i = 0$, the inequality (3.7) reduces to $|\mathbf{w}_i|^p \geq 0$, and surely holds since $\text{signQ}(\mathbf{v}_i^{(\gamma)}) = 0$ according the definition (2.5b) (and under the assumption $0^0 = 1$). The equality in (3.7) holds when $\mathbf{w}_i = \mathbf{v}_i$. Summing up (3.7) together, we obtain

$$\begin{aligned} &\sum_{i=1}^n \left(\sqrt{\sum_{j=0}^3 (w_i^{(j)})^2} \right)^p \\ &\geq p \sum_{i=1}^n \left[|\mathbf{v}_i|^{p-1} \cdot (\text{signQ}(\mathbf{v}_i^{(\gamma)}))^T \mathbf{w}_i^{(\gamma)} \right] \\ &\quad + (1-p) \sum_{i=1}^n \left(\sqrt{\sum_{j=0}^3 (v_i^{(j)})^2} \right)^p. \end{aligned}$$

Consequently, (3.3) holds and the inequality becomes equality when $\mathbf{w} = \mathbf{v}$ no matter \mathbf{v} has zero entries or not. This completes the proof. \square

Let $w \in \mathbb{R}^n$, $v \in \mathbb{R}^n$, and $p, q \in [1, \infty]$ be two scalars with $1/p + 1/q = 1$. Then the Hölder's inequality [46] states that

$$\sum_{i=1}^n |v_i w_i| \leq \|v\|_q \|w\|_p. \quad (3.8)$$

The equality holds if and only if there exists a positive real scalar c satisfying $|w_i|^p = c |v_i|^q, i = 1, 2, \dots, n$. Since two arbitrary quaternions are not comparable, here we consider the linear optimization problem with L_p -norm based on the Hölder's inequality.

LEMMA 3.2. *Let $\mathbf{w} \in \mathbb{Q}^n$, $\mathbf{v} \in \mathbb{Q}^n \setminus \{0\}$, and let $p, q \in [1, \infty]$ be two scalars satisfying $1/p + 1/q = 1$. Then the quaternion optimization problem*

$$\max_{\mathbf{w}} \mathbf{v}^* \mathbf{w}, \text{ s.t. } \|\mathbf{w}\|_p^p = 1 \quad (3.9)$$

has a closed-form solution

$$\mathbf{w}^{(\gamma)} = \frac{|\mathbf{v}^{(\gamma)}|_Q^{q-1}}{\|\mathbf{v}^{(\gamma)}\|_{2,q}^{q-1}} \circ \text{signQ}(\mathbf{v}^{(\gamma)}).$$

Proof. According to the representation (2.4), the quaternion optimization problem (3.9) is equivalently rewritten to

$$\max_{\mathbf{w}^{(\gamma)}} (\mathbf{v}^{(\gamma)})^T \mathbf{w}^{(\gamma)}, \quad s.t. \quad \|\mathbf{w}^{(\gamma)}\|_{2,p}^p = 1.$$

Based on the Hölder's inequality (3.8), we have

$$\begin{aligned} (\mathbf{v}^{(\gamma)})^T \mathbf{w}^{(\gamma)} &\leq \sum_{i=1}^n \sum_{j=0}^3 |v_i^{(j)} w_i^{(j)}| \leq \sum_{i=1}^n |\mathbf{v}_i| |\mathbf{w}_i| = |\mathbf{v}|^T |\mathbf{w}| \\ &\leq \|\mathbf{v}\|_q \|\mathbf{w}\|_p = \|\mathbf{v}^{(\gamma)}\|_{2,q} \|\mathbf{w}^{(\gamma)}\|_{2,p} = \|\mathbf{v}^{(\gamma)}\|_{2,q}. \end{aligned}$$

Therefore, the maximum of the objective function is obtained when the inequalities become equalities. The equality

in $(\mathbf{v}^{(\gamma)})^T \mathbf{w}^{(\gamma)} \leq \sum_{i=1}^n \sum_{j=0}^3 |v_i^{(j)} w_i^{(j)}|$ holds when

$$\text{sign}(v_i^{(j)}) = \text{sign}(w_i^{(j)}).$$

The equality in $\sum_{i=1}^n \sum_{j=0}^3 |v_i^{(j)} w_i^{(j)}| \leq \sum_{i=1}^n |\mathbf{v}_i| |\mathbf{w}_i|$ holds when

$$|w_i^{(j)}|^2 = c_i |v_i^{(j)}|^2, \quad j = 0, 1, 2, 3. \quad (3.10)$$

If $\mathbf{v}_i = 0$, we set $c_i = 0$ and $w_i^{(j)} = 0$. If $\mathbf{v}_i \neq 0$, then the constant c_i is calculated by

$$c_i = \frac{\sum_{j=0}^3 |w_i^{(j)}|^2}{\sum_{j=0}^3 |v_i^{(j)}|^2} = \frac{|\mathbf{w}_i|^2}{|\mathbf{v}_i|^2}. \quad (3.11)$$

Inputting (3.11) into (3.10) yields the expression

$$|w_i^{(j)}| = \left(c_i |v_i^{(j)}|^2 \right)^{\frac{1}{2}} = \frac{|\mathbf{w}_i|}{|\mathbf{v}_i|} |v_i^{(j)}|. \quad (3.12)$$

Then we have

$$\begin{aligned} w_i^{(j)} &= \frac{|\mathbf{w}_i|}{|\mathbf{v}_i|} |v_i^{(j)}| \text{sign}(v_i^{(j)}), \quad \text{if } \mathbf{v}_i \neq 0; \\ w_i^{(j)} &= 0, \quad \text{if } \mathbf{v}_i = 0. \end{aligned} \quad (3.13)$$

For simplicity, we introduce an auxiliary variable $Y^{\mathbf{w}}$ to denote the absolute of quaternion vector \mathbf{w} . The equality in $|\mathbf{v}|^T |\mathbf{w}| \leq \|\mathbf{v}\|_q \|\mathbf{w}\|_p$ holds when

$$|Y_i^{\mathbf{w}}|^p = c |Y_i^{\mathbf{v}}|^q, \quad i = 1, 2, \dots, n. \quad (3.14)$$

Since $\mathbf{v} \neq 0$, the constant c is then calculated by

$$c = \frac{\|Y^{\mathbf{w}}\|_p^p}{\|Y^{\mathbf{v}}\|_q^q} = \frac{\|\mathbf{w}^{(\gamma)}\|_{2,p}^p}{\|\mathbf{v}^{(\gamma)}\|_{2,q}^q} = \frac{1}{\|\mathbf{v}^{(\gamma)}\|_{2,q}^q}. \quad (3.15)$$

Substituting (3.15) into (3.14), we have

$$|Y_i^{\mathbf{w}}| = (c |Y_i^{\mathbf{v}}|^q)^{1/p} = \frac{|Y_i^{\mathbf{v}}|^{q-1}}{\|Y^{\mathbf{v}}\|_q^{q-1}}, \quad i = 1, 2, \dots, n,$$

i.e.

$$\|\mathbf{w}_i\|_2 = \frac{\|\mathbf{v}_i\|_2^{q-1}}{\|\mathbf{v}^{(\gamma)}\|_{2,q}^{q-1}}.$$

Together with equality (3.13), we obtain the expression

$$\begin{aligned} w_i^{(j)} &= \frac{\|\mathbf{v}_i\|_2^{q-1}}{\|\mathbf{v}^{(\gamma)}\|_{2,q}^{q-1}} \frac{1}{\|\mathbf{v}_i\|_2} |v_i^{(j)}| \text{sign}(v_i^{(j)}) \\ &= \frac{|\mathbf{v}_i|^{q-1}}{\|\mathbf{v}^{(\gamma)}\|_{2,q}^{q-1}} \frac{v_i^{(j)}}{|\mathbf{v}_i|}. \end{aligned}$$

Connecting to the definitions in (2.5) and rewriting the equation into vector form, we yields the desired result

$$\mathbf{w}^{(\gamma)} = \frac{|\mathbf{v}^{(\gamma)}|_Q^{q-1}}{\|\mathbf{v}^{(\gamma)}\|_{2,q}^{q-1}} \circ \text{sign} \mathbf{Q}(\mathbf{v}^{(\gamma)}).$$

The proof is completed. \square

LEMMA 3.3. Let $\mathbf{w} = [\mathbf{w}_i]$, $\mathbf{v} = [\mathbf{v}_i] \in \mathbb{Q}^n$ with $\mathbf{w}_i \neq 0$ and $\mathbf{v}_i \neq 0$ for any $1 \leq i \leq n$, and $0 < p < 1$. Then

$$\|\mathbf{w}\|_p^p \leq p(|\mathbf{v}|^{p-1})^T |\mathbf{w}| + (1-p) \|\mathbf{v}\|_p^p$$

holds wherein the inequality becomes equality when $|\mathbf{w}| = |\mathbf{v}|$.

Proof. Recall that the absolute value function is defined in (2.1a). For any quaternion vector \mathbf{w} with each entry $\mathbf{w}_i \neq 0$, $|\mathbf{w}|$ is a real vector with positive entries. Let $f(|\mathbf{w}|) = \|\mathbf{w}\|_p^p$, then $f(\cdot)$ is non-convex and differentiable at positive real vector when $0 < p < 1$. From the first-order convexity condition (7.4), we have

$$f(|\mathbf{w}|) \leq f(|\mathbf{v}|) + \nabla f(|\mathbf{v}|)^T (|\mathbf{w}| - |\mathbf{v}|),$$

and

$$\begin{aligned} \nabla f(|\mathbf{v}|) &= \nabla \|\mathbf{v}\|_p^p = \frac{\partial \|\mathbf{v}\|_p^p}{\partial |\mathbf{v}|} \Big|_{\mathbf{w}=\mathbf{v}} \\ &= p |\mathbf{v}|^{p-1} \circ \text{sign}(|\mathbf{v}|). \end{aligned}$$

Therefore,

$$f(|\mathbf{w}|) \leq \|\mathbf{v}\|_p^p + [p |\mathbf{v}|^{p-1} \circ \text{sign}(|\mathbf{v}|)]^T |\mathbf{w}| - p \|\mathbf{v}\|_p^p.$$

Thus, we obtain $\|\mathbf{w}\|_p^p \leq p [|\mathbf{v}|^{p-1} \circ \text{sign}(|\mathbf{v}|)]^T |\mathbf{w}| + (1-p) \|\mathbf{v}\|_p^p$. Apparently, if $\mathbf{w}^{(\gamma)} = \mathbf{v}^{(\gamma)}$, it must satisfy the condition that $|\mathbf{w}| = |\mathbf{v}|$. \square

Note that in our method, in order to meet the condition that $\mathbf{w}_i \neq 0$, if any element in the projection vector $(\mathbf{w}^{(\gamma)})^{(k)}$ is zero, then we replace it with $(\mathbf{w}^{(\gamma)})^{(k)} + \varepsilon$, where ε is a random scalar that is sufficiently close to zero. In the rest of this section, we always assume that the mean of the training set is zero, that is, $\Psi = 0$; otherwise, we centralize the training samples by $\mathbf{F}_i = \mathbf{F}_i - \Psi$, $i = 1, \dots, \ell$.

3.1.1 Case 1: Convex constraint set

Now, we proceed to the solution of G2DQPCA problem for the first case, i.e., $p \geq 1$, based on Theorem 3.1 and Lemma 3.2.

The quaternion optimization problem of G2DQPCA states

$$\max_{\mathbf{w}} \sum_{i=1}^{\ell} \|\mathbf{F}_i \mathbf{w}\|_s^s, \quad s.t. \quad \|\mathbf{w}\|_p^p = 1, \quad (3.16)$$

where $s \geq 1, p \geq 1, \mathbf{w} \in \mathbb{Q}^n$. The constraint set is convex. According to definitions (2.3) and (2.4), the quaternion optimization problem (3.16) can be transformed to its equivalent real counterpart,

$$\max_{\mathbf{w}^{(\gamma)}} \sum_{i=1}^{\ell} \|\mathbf{F}_i^{(\gamma)} \mathbf{w}^{(\gamma)}\|_{2,s}^s, \quad s.t. \quad \|\mathbf{w}^{(\gamma)}\|_p^p = 1. \quad (3.17)$$

This real optimization problem can be turned into iteratively maximizing a surrogate function under the MM framework, as shown below. Assume $(\mathbf{w}^{(\gamma)})^{(k)}$ is the projection vector at the k -th step in the iteration procedure. It can be regarded

as a constant vector that is irrelevant with respect to $\mathbf{w}^{(\gamma)}$. Define

$$\hat{F}_i = |\mathbf{F}_i^{(\gamma)}(\mathbf{w}^{(\gamma)})^{(k)}|_Q^{s-1} \circ \text{signQ}(\mathbf{F}_i^{(\gamma)}(\mathbf{w}^{(\gamma)})^{(k)}),$$

according to Theorem 3.1. The convex objective function can be linearized as

$$\begin{aligned} \sum_{i=1}^{\ell} \|\mathbf{F}_i \mathbf{w}\|_s^s &= \sum_{i=1}^{\ell} \|\mathbf{F}_i^{(\gamma)} \mathbf{w}^{(\gamma)}\|_{2,s}^s \\ &\geq s \sum_{i=1}^{\ell} \hat{F}_i^T \mathbf{F}_i^{(\gamma)} \mathbf{w}^{(\gamma)} + (1-s) \sum_{i=1}^{\ell} \|\mathbf{F}_i^{(\gamma)}(\mathbf{w}^{(\gamma)})^{(k)}\|_{2,s}^s, \end{aligned}$$

wherein the inequality becomes equality when $\mathbf{w}^{(\gamma)} = (\mathbf{w}^{(\gamma)})^{(k)}$. Denote the objective function by $f(\mathbf{w}^{(\gamma)})$, and the linearized function by $g(\mathbf{w}^{(\gamma)} | (\mathbf{w}^{(\gamma)})^{(k)})$. That is

$$f(\mathbf{w}^{(\gamma)}) = \sum_{i=1}^{\ell} \|\mathbf{F}_i^{(\gamma)} \mathbf{w}^{(\gamma)}\|_{2,s}^s,$$

and

$$\begin{aligned} g(\mathbf{w}^{(\gamma)} | (\mathbf{w}^{(\gamma)})^{(k)}) &= s \sum_{i=1}^{\ell} \hat{F}_i^T \mathbf{F}_i^{(\gamma)} \mathbf{w}^{(\gamma)} \\ &+ (1-s) \sum_{i=1}^{\ell} \|\mathbf{F}_i^{(\gamma)}(\mathbf{w}^{(\gamma)})^{(k)}\|_{2,s}^s. \end{aligned} \quad (3.18)$$

According to (3.5) and by simple algebra, it is easy to verify that

$$\hat{F}_i^T \mathbf{F}_i^{(\gamma)}(\mathbf{w}^{(\gamma)})^{(k)} = \|\mathbf{F}_i^{(\gamma)}(\mathbf{w}^{(\gamma)})^{(k)}\|_{2,s}^s.$$

Then we have $f((\mathbf{w}^{(\gamma)})^{(k)}) = g((\mathbf{w}^{(\gamma)})^{(k)} | (\mathbf{w}^{(\gamma)})^{(k)})$ and $f(\mathbf{w}^{(\gamma)}) \geq g(\mathbf{w}^{(\gamma)} | (\mathbf{w}^{(\gamma)})^{(k)})$ for all $\mathbf{w}^{(\gamma)}$, satisfying the two key conditions of the minorization-maximization (MM) framework [42]. Therefore, $g(\mathbf{w}^{(\gamma)} | (\mathbf{w}^{(\gamma)})^{(k)})$ is a feasible surrogate function of $f(\mathbf{w}^{(\gamma)})$. According to the MM framework, the optimization problem in (3.16) can be turned into iteratively maximizing the surrogate function as follows

$$\begin{aligned} (\mathbf{w}^{(\gamma)})^{(k+1)} &= \arg \max_{\mathbf{w}^{(\gamma)}} g(\mathbf{w}^{(\gamma)} | (\mathbf{w}^{(\gamma)})^{(k)}), \\ \text{s.t. } \|\mathbf{w}^{(\gamma)}\|_{2,p}^p &= 1. \end{aligned}$$

Define

$$(\mathbf{v}^{(\gamma)})^{(k)} = \sum_{i=1}^{\ell} (\mathbf{F}_i^{(\gamma)})^T \hat{F}_i, \quad (3.19)$$

by dropping the term irrelevant to $\mathbf{w}^{(\gamma)}$ in the surrogate function (3.18), maximizing the surrogate function leads to a linear optimization problem with L_p -norm constraint

$$\begin{aligned} (\mathbf{w}^{(\gamma)})^{(k+1)} &= \arg \max_{\mathbf{w}^{(\gamma)}} [(\mathbf{v}^{(\gamma)})^{(k)}]^T \mathbf{w}^{(\gamma)}, \\ \text{s.t. } \|\mathbf{w}^{(\gamma)}\|_{2,p}^p &= 1. \end{aligned} \quad (3.20)$$

According to Lemma 3.2, the solution of this problem is

$$(\mathbf{w}^{(\gamma)})^{(k+1)} = \frac{|(\mathbf{v}^{(\gamma)})^{(k)}|_Q^{q-1}}{\|(\mathbf{v}^{(\gamma)})^{(k)}\|_{2,q}^{q-1}} \circ \text{signQ}((\mathbf{v}^{(\gamma)})^{(k)}), \quad (3.21)$$

where q satisfies $\frac{1}{p} + \frac{1}{q} = 1$. The solution is rewritten in a two-step procedure as

$$\begin{aligned} (\mathbf{u}^{(\gamma)})^{(k)} &= |(\mathbf{v}^{(\gamma)})^{(k)}|_Q^{q-1} \circ \text{signQ}((\mathbf{v}^{(\gamma)})^{(k)}), \\ (\mathbf{w}^{(\gamma)})^{(k+1)} &= \frac{(\mathbf{u}^{(\gamma)})^{(k)}}{\|(\mathbf{u}^{(\gamma)})^{(k)}\|_{2,p}}. \end{aligned} \quad (3.22)$$

Two extreme conditions of case 1, i.e., $p = 1$ and $p = \infty$ are discussed as follows. When $p = 1$, we will have $q = \infty$ according to the relation $1/p + 1/q = 1$. Then the denominator of (3.21) becomes $\|(\mathbf{v}^{(\gamma)})^{(k)}\|_{2,\infty}$. Let $j = \arg \max_{i=1,\dots,n} |\mathbf{v}_i^{(k)}|$, i.e., $|\mathbf{v}_j^{(k)}|$ is the largest value in $|\mathbf{v}^{(k)}|$. By taking the limit of (3.21) we have

$$\mathbf{w}_i^{(k+1)} = \begin{cases} \text{sign}(\mathbf{v}_i^{(k)}), & i = j, \\ 0, & i \neq j, \end{cases} \quad (3.23)$$

for $i = 1, 2, \dots, n$. Similarly, when p approaches infinity, the limit of (3.21) is

$$(\mathbf{w}^{(\gamma)})^{(k+1)} = \text{signQ}((\mathbf{v}^{(\gamma)})^{(k)}). \quad (3.24)$$

3.1.2 Case 2: Non-convex constraint set

When $0 < p < 1$, the constraint set becomes non-convex. With introducing an auxiliary variable $Y^{\mathbf{w}} \equiv |\mathbf{w}|$, the L_p -norm

$$\|\mathbf{w}\|_p^p = \|Y^{\mathbf{w}}\|_p^p, \quad (3.25)$$

and clearly $Y^{\mathbf{w}} \in \mathbb{R}^n, Y^{\mathbf{w}} \geq 0$.

Here we try to apply the method of Lagrange multipliers, considering that the constraint set is non-convex and non-Lipschitz continuous. Maximizing the optimization problem of function (3.1) equals to maximizing the Lagrangian as follows

$$\max_{\mathbf{w}} \sum_{i=1}^{\ell} \|\mathbf{F}_i \mathbf{w}\|_s^s - \lambda (\|\mathbf{w}\|_p^p - 1), \quad (3.26)$$

where $s \geq 1, 0 < p < 1, \lambda > 0, \mathbf{w} \in \mathbb{Q}^n$.

Same as in Case 1, we firstly translate this function according to (3.17) and (3.25) into

$$\max_{\mathbf{w}^{(\gamma)}} \sum_{i=1}^{\ell} \|\mathbf{F}_i^{(\gamma)} \mathbf{w}^{(\gamma)}\|_{2,s}^s - \lambda (\|Y^{\mathbf{w}}\|_p^p - 1),$$

where $\|Y^{\mathbf{w}}\|_p^p = \|\mathbf{w}^{(\gamma)}\|_{2,p}^p$ is essentially a function related to $\mathbf{w}^{(\gamma)}$. Again, the problem is transformed into iteratively maximizing a surrogate function under the MM framework. Assume that $(\mathbf{w}^{(\gamma)})^{(k)}$ is the projection vector at the k -th step in the iteration procedure. If any element in $(\mathbf{w}^{(\gamma)})^{(k)}$ is zero, then we replace it with $(\mathbf{w}^{(\gamma)})^{(k)} + \varepsilon$ to make sure that it has no zero elements, where ε is a random scalar that is sufficiently close to zero. According to Theorem 3.1 and Lemma 3.3, we have

$$\begin{aligned} \sum_{i=1}^{\ell} \|\mathbf{F}_i^{(\gamma)} \mathbf{w}^{(\gamma)}\|_{2,s}^s - \lambda (\|Y^{\mathbf{w}}\|_p^p - 1) &\geq s((\mathbf{v}^{(\gamma)})^{(k)})^T \mathbf{w}^{(\gamma)} \\ &+ (1-s) \sum_{i=1}^{\ell} \|\mathbf{F}_i^{(\gamma)}(\mathbf{w}^{(\gamma)})^{(k)}\|_{2,s}^s - \lambda(1-p) \|\mathbf{w}^{(k)}\|_p^p \\ &- \lambda p (|\mathbf{w}^{(k)}|^{p-1} \circ \text{sign}(|\mathbf{w}^{(k)}|))^T Y^{\mathbf{w}} + \lambda, \end{aligned}$$

where $(\mathbf{v}^{(\gamma)})^{(k)}$ is defined in (3.19),

$$|\mathbf{w}^{(k)}| = \begin{bmatrix} |\mathbf{w}_1^{(k)}| & |\mathbf{w}_2^{(k)}| & \dots & |\mathbf{w}_n^{(k)}| \end{bmatrix}^T,$$

and this inequality becomes equality when $\mathbf{w}^{(\gamma)} = (\mathbf{w}^{(\gamma)})^{(k)}$. Denote the left-hand side of the inequality by $f(\mathbf{w}^{(\gamma)})$ and the right-hand side by $g(\mathbf{w}^{(\gamma)} | (\mathbf{w}^{(\gamma)})^{(k)})$, i.e.,

$$f(\mathbf{w}^{(\gamma)}) = \sum_{i=1}^{\ell} \|\mathbf{F}_i^{(\gamma)} \mathbf{w}^{(\gamma)}\|_{2,s}^s - \lambda (\|Y^{\mathbf{w}}\|_p^p - 1), \quad (3.27)$$

and

$$\begin{aligned} g(\mathbf{w}^{(\gamma)} | (\mathbf{w}^{(\gamma)})^{(k)}) &= s((\mathbf{v}^{(\gamma)})^{(k)})^T \mathbf{w}^{(\gamma)} \\ &+ (1-s) \sum_{i=1}^{\ell} \|\mathbf{F}_i^{(\gamma)} (\mathbf{w}^{(\gamma)})^{(k)}\|_{2,s}^s - \lambda(1-p) \|\mathbf{w}^{(k)}\|_p^p \\ &- \lambda p (|\mathbf{w}^{(k)}|^{p-1} \circ \text{sign}(|\mathbf{w}^{(k)}|))^T Y^{\mathbf{w}} + \lambda. \end{aligned}$$

By the simple algebraic calculation, we obtain

$$f((\mathbf{w}^{(\gamma)})^{(k)}) = g((\mathbf{w}^{(\gamma)})^{(k)} | (\mathbf{w}^{(\gamma)})^{(k)})$$

and

$$f(\mathbf{w}^{(\gamma)}) \geq g(\mathbf{w}^{(\gamma)} | (\mathbf{w}^{(\gamma)})^{(k)})$$

for all $\mathbf{w}^{(\gamma)}$, which satisfy the two key conditions of the MM framework. Therefore, $g(\mathbf{w}^{(\gamma)} | (\mathbf{w}^{(\gamma)})^{(k)})$ is a feasible surrogate function of $f(\mathbf{w}^{(\gamma)})$. According to the MM framework, the optimization problem in (3.26) can be turned into iteratively maximizing the surrogate function as follows

$$(\mathbf{w}^{(\gamma)})^{(k+1)} = \arg \max_{\mathbf{w}^{(\gamma)}} g(\mathbf{w}^{(\gamma)} | (\mathbf{w}^{(\gamma)})^{(k)}).$$

Then the following quadratic optimization problem will be reached after ignoring irrelevant terms of $\mathbf{w}^{(\gamma)}$

$$\begin{aligned} (\mathbf{w}^{(\gamma)})^{(k+1)} &= \arg \max_{\mathbf{w}^{(\gamma)}} s((\mathbf{v}^{(\gamma)})^{(k)})^T \mathbf{w}^{(\gamma)} \\ &- \lambda p (|\mathbf{w}^{(k)}|^{p-1} \circ \text{sign}(|\mathbf{w}^{(k)}|))^T Y^{\mathbf{w}}. \end{aligned} \quad (3.28)$$

Let $h(\mathbf{w}^{(\gamma)}) = s((\mathbf{v}^{(\gamma)})^{(k)})^T \mathbf{w}^{(\gamma)} - \lambda p (\hat{\mathbf{w}}^{(k)})^T Y^{\mathbf{w}}$, where $\hat{\mathbf{w}}^{(k)} = |\mathbf{w}^{(k)}|^{p-1} \circ \text{sign}(|\mathbf{w}^{(k)}|)$ and $Y^{\mathbf{w}}$ is defined in (3.25). Now we consider the partial derivative with respect to $\mathbf{w}^{(\gamma)}$

$$\begin{aligned} \left[\frac{\partial h(\mathbf{w}^{(\gamma)})}{\partial \mathbf{w}^{(\gamma)}} \right]_l &= \frac{\partial h(\mathbf{w}^{(\gamma)})}{\partial w_i^{(j)}} \\ &= s(\mathbf{v}^{(k)})_i^{(j)} - \lambda p \left[|\mathbf{w}_i^{(k)}|^{p-1} \frac{w_i^{(j)}}{|\mathbf{w}_i^{(k)}|} \right], \end{aligned} \quad (3.29)$$

where $i = 1, 2, \dots, n$, $j = 0, 1, 2, 3$ and $l = 1, 2, \dots, 4n$.

Let the above equation equal to zero and we get

$$w_i^{(j)} = \frac{s}{\lambda p} (\mathbf{v}^{(k)})_i^{(j)} |\mathbf{w}_i^{(k)}| |\mathbf{w}_i^{(k)}|^{1-p}.$$

Rewrite the component as vector expression which is the solution of the problem (3.28)

$$(\mathbf{w}^{(\gamma)})^{(k+1)} = \frac{s}{\lambda p} (\mathbf{v}^{(\gamma)})^{(k)} \circ \tilde{\mathbf{w}}^{(\gamma)},$$

where $\tilde{\mathbf{w}}^{(\gamma)} = |\mathbf{w}^{(\gamma)}|_Q \circ |(\mathbf{w}^{(\gamma)})^{(k)}|_Q^{1-p}$. Considering the constraint $\|\mathbf{w}\|_p^p = 1$, i.e. $\|\mathbf{w}^{(\gamma)}\|_{2,p}^p = 1$ and $\lambda > 0$, we have

$$\lambda = \frac{s}{p} \|(\mathbf{v}^{(\gamma)})^{(k)} \circ \tilde{\mathbf{w}}^{(\gamma)}\|_{2,p}.$$

Then the update rule is

$$(\mathbf{w}^{(\gamma)})^{(k+1)} = \frac{(\mathbf{v}^{(\gamma)})^{(k)} \circ \tilde{\mathbf{w}}^{(\gamma)}}{\|(\mathbf{v}^{(\gamma)})^{(k)} \circ \tilde{\mathbf{w}}^{(\gamma)}\|_{2,p}}. \quad (3.30)$$

The above solution equals to the two-step procedure as below

$$(\mathbf{u}^{(\gamma)})^{(k)} = (\mathbf{v}^{(\gamma)})^{(k)} \circ \tilde{\mathbf{w}}^{(\gamma)}, \quad (3.31)$$

$$(\mathbf{w}^{(\gamma)})^{(k+1)} = \frac{(\mathbf{u}^{(\gamma)})^{(k)}}{\|(\mathbf{u}^{(\gamma)})^{(k)}\|_{2,p}}. \quad (3.32)$$

This completes the solution in Case 2.

Now we have obtained the solution of the quaternion optimization problem of G2DQPCA. From the results in (3.21) and (3.30), we observe that a closed-form solution is obtained in each iteration for both cases.

REMARK 3.1. G2DQPCA is a generalization of 2DQPCA with applying L_p -norm both in the objective function and the constraint function. Let $s = p = 2$ then G2DQPCA reduces to 2DQPCA [1], [2],

$$\begin{aligned} \arg \max_{\mathbf{w}_1, \dots, \mathbf{w}_r \in \mathbb{Q}^n} & \sum_{j=1}^r \sum_{i=1}^{\ell} \|\mathbf{F}_i \mathbf{w}_j\|_2^2, \\ \text{s.t.} & \begin{cases} \mathbf{w}_j^* \mathbf{w}_i = \|\mathbf{w}_j\|_2^2 = 1 & (i = j), \\ \mathbf{w}_j^* \mathbf{w}_i = 0 & (i \neq j). \end{cases} \end{aligned} \quad (3.33)$$

Indeed, let $\mathbf{W} = [\mathbf{w}_1, \dots, \mathbf{w}_r]$ then

$$\begin{aligned} \arg \max_{\mathbf{w}_1, \dots, \mathbf{w}_r \in \mathbb{Q}^n} & \sum_{j=1}^r \sum_{i=1}^{\ell} \|\mathbf{F}_i \mathbf{w}_j\|_2^2 = \arg \max_{\mathbf{W} \in \mathbb{Q}^{n \times k}} \sum_{i=1}^{\ell} \|\mathbf{F}_i \mathbf{W}\|_F^2 \\ &= \arg \min_{\mathbf{W} \in \mathbb{Q}^{n \times k}} \sum_{i=1}^{\ell} \|\mathbf{F}_i (\mathbf{I} - \mathbf{W} \mathbf{W}^*)\|_F^2. \end{aligned}$$

The ridge regression model [3] of 2DQPCA is equivalent to the quaternion optimization model (3.33). Notice that the Frobenius norm of a quaternion matrix \mathbf{A} is defined by $\|\mathbf{A}\|_F^2 = \text{trace}(\mathbf{A}^* \mathbf{A}) = \text{trace}(\mathbf{A} \mathbf{A}^*)$.

REMARK 3.2. G2DQPCA generalizes G2DPCA from the real field to the quaternion skew-field. Compared with G2DPCA, we firstly constrain the orthogonality of the projection vectors, $\mathbf{w}_i, i = 1, 2, \dots, r$, in the ridge regression model (3.1). We will elaborate this constraint later.

3.2 A new quaternion optimization algorithm with deflation

Now assume we have obtained the first r projection vectors, i.e., $\mathbf{W} = [\mathbf{w}_1, \mathbf{w}_2, \dots, \mathbf{w}_r]$, where $1 \leq r < n$. The $(r+1)$ -th projection vector \mathbf{w}_{r+1} can be calculated similarly on the deflated samples

$$\mathbf{F}_i^{\text{deflated}} = \mathbf{F}_i (\mathbf{I} - \mathbf{W} \mathbf{W}^*), i = 1, 2, \dots, \ell. \quad (3.34)$$

What is particularly noteworthy is that the projection vector \mathbf{w}_{r+1} obtained at each iteration must be orthonormalized against all previous $\mathbf{w}_i, i = 1, 2, \dots, r$ by a standard Gram-Schmidt procedure in quaternion domain. This is because when we completed deflation in the r -th direction that means there is no information left in this direction and then projection on the deflated samples should be zero. We observe that after r steps each sample is transformed into (3.34). After deflating samples by r directions, we obtain that

$$\mathbf{F}_i^{\text{deflated}} \mathbf{w}_j = \mathbf{F}_i (\mathbf{I} - \mathbf{W} \mathbf{W}^*) \mathbf{w}_j, \quad (3.35)$$

where $j = 1, 2, \dots, r+1$. $\mathbf{F}_i^{\text{deflated}} \mathbf{w}_j$ should be zero if $j = 1, 2, \dots, r$. Otherwise the feature information can be lost because of the interference from other direction. From (3.35) with $j = r+1$, we also know that the $(r+1)$ -th projector must not be linearly represented by the prior projectors, or in other words, the newly computed projector is not in the subspace generated by the known projectors, so that we orthogonalize the computed projector to the known ones.

Algorithm 1 G2DQPCA: the generalized two-dimensional quaternion principal component analysis

Require: Training samples $\mathbf{F}_1, \mathbf{F}_2, \dots, \mathbf{F}_\ell$, the number of selected feature r , and parameters $s \in [1, \infty), p \in (0, \infty]$.

Ensure: Optimal quaternion projection matrix \mathbf{W} , and weighted coefficient vector \mathbf{D}

- 1: Initialize $\mathbf{W} = [], \mathbf{D} = [], \mathbf{F}_i^0 = \mathbf{F}_i$.
- 2: **for** $t = 1, 2, \dots, r$ **do**
- 3: Initialize $k = 0, \delta = 1$, arbitrary $\mathbf{w}^{(0)}$ with $\|\mathbf{w}^{(0)}\|_p = 1$.
- 4: $f^{(0)} = \sum_{i=1}^{\ell} \|\mathbf{F}_i \mathbf{w}^{(0)}\|_s$.
- 5: **while** $\delta > 10^{-4}$ **do**
- 6: $\mathbf{v}^{(k)} = \sum_{i=1}^{\ell} \mathbf{F}_i^* [|\mathbf{F}_i \mathbf{w}^{(k)}|^{s-1} \odot \text{sign}(\mathbf{F}_i \mathbf{w}^{(k)})]$.
- 7: **if** $0 < p < 1$ **then**
- 8: $\mathbf{u}^{(k)} = |\mathbf{w}^{(0)}| \odot |\mathbf{w}^{(k)}|^{1-p} \odot \mathbf{v}^{(k)}$,
- 9: $\mathbf{w}^{(k+1)} = \frac{\mathbf{u}^{(k)}}{\|\mathbf{u}^{(k)}\|_p}$.
- 10: **else if** $p = 1$ **then**
- 11: $j = \arg \max_{1 \leq i \leq n} |\mathbf{v}_i^{(k)}|$,
- 12: $\mathbf{w}_i^{(k+1)} = \begin{cases} \text{sign}(\mathbf{v}_j^{(k)}), & i = j, \\ 0, & i \neq j. \end{cases}$
- 13: **else if** $1 < p < \infty$ **then**
- 14: $q = p/(p-1)$,
- 15: $\mathbf{u}^{(k)} = |\mathbf{v}^{(k)}|^{q-1} \odot \text{sign}(\mathbf{v}^{(k)})$,
- 16: $\mathbf{w}^{(k+1)} = \frac{\mathbf{u}^{(k)}}{\|\mathbf{u}^{(k)}\|_p}$.
- 17: **else if** $p = \infty$ **then**
- 18: $\mathbf{w}^{(k+1)} = \text{sign}(\mathbf{v}^{(k)})$.
- 19: **end if**
- 20: $f^{(k+1)} = \sum_{i=1}^{\ell} \|\mathbf{F}_i \mathbf{w}^{(k+1)}\|_s$.
- 21: $\delta = |f^{(k+1)} - f^{(k)}| / |f^{(k)}|$.
- 22: $k \leftarrow k + 1$.
- 23: **end while**
- 24: $\mathbf{w}_t = \mathbf{w}^{(k)}$.
- 25: Orthogonalize \mathbf{w}_t with the previous vector \mathbf{w}_i by quaternion QR factorization.
- 26: $f^{(t)} = \sum_{i=1}^{\ell} \|\mathbf{F}_i \mathbf{w}_t\|_s$.
- 27: $\mathbf{W} \leftarrow [\mathbf{W}, \mathbf{w}_t]$.
- 28: $\mathbf{D} \leftarrow [\mathbf{D}, f^{(t)}]$.
- 29: $\mathbf{F}_i = \mathbf{F}_i^0 (\mathbf{I} - \mathbf{W} \mathbf{W}^*), i = 1, 2, \dots, \ell$.
- 30: **end for**

Another notable feature here is the usage of deflation in general. It should not be used to compute more than a few projection vectors because of the fact that the simple matrix F_i will accumulate errors from all previous computations and this can be disastrous if the cases where cancellations

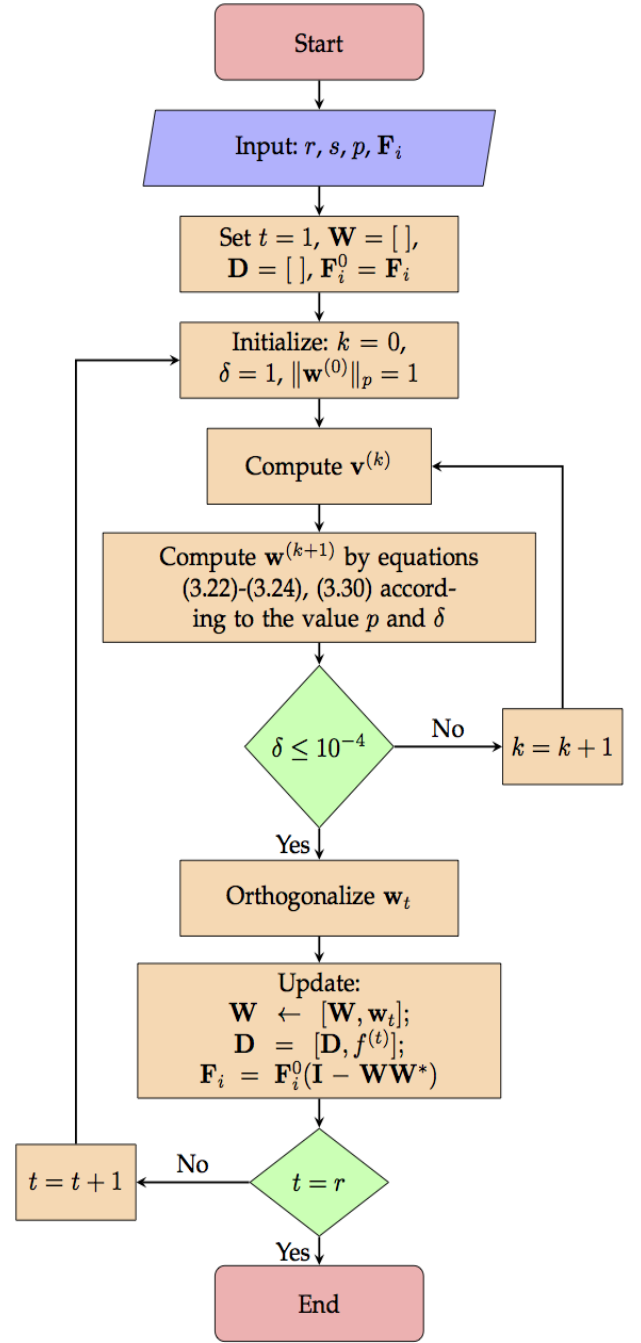


Fig. 2: Flowchart of Algorithm 1

are so severe in the orthogonalization steps. In our experiments, we use quaternion QR Factorization [45] to complete such orthogonalizing process.

We summarize the above steps into Algorithm 1. Here the notation \odot is defined by multiplying the corresponding real coefficients between two quaternions. For example, assume $\mathbf{w} = w_0 + w_1\mathbf{i} + w_2\mathbf{j} + w_3\mathbf{k}$, $\mathbf{v} = v_0 + v_1\mathbf{i} + v_2\mathbf{j} + v_3\mathbf{k}$, then

$$\mathbf{w} \odot \mathbf{v} = (w_0 \circ v_0) + (w_1 \circ v_1)\mathbf{i} + (w_2 \circ v_2)\mathbf{j} + (w_3 \circ v_3)\mathbf{k}.$$

The flowchart of Algorithm 1 is shown in Figure 2.

4 COLOR IMAGE ANALYSIS WITH WEIGHTED PROJECTION

In this section, we present the weighted G2DQPCA algorithm for color image recognition and the G2DQPCA algorithm for the low-rank reconstructions of a group of color images.

With applying Algorithm 1 to the training data in color image recognition, we obtain r pairs of optimal values and projection vectors, denoted by $(f^{(1)}, \mathbf{w}_1), \dots, (f^{(r)}, \mathbf{w}_r)$. The contributions of $\mathbf{w}_1, \dots, \mathbf{w}_r$ to increase the recognition rate can be characterized by $f^{(1)}, \dots, f^{(r)}$. Let $t = 1, \dots, r$. It is not difficult to find out that when $s = p = 2$, the value of $f^{(t)}$ is equal to the t -th eigenvalue of the covariance matrix of training set, which represents the variance on the direction \mathbf{w}_t . In practical implementation, we normalize $f^{(t)}$ by $f^{(t)} / \sum_{t=1}^r f^{(t)}$ and weight each projection vector \mathbf{w}_t by multiplying the normalized $f^{(t)}$.

A new weighted G2DQPCA algorithm can be proposed for color image recognition with using the weighted projection vectors $\mathbf{w}_1 f^{(1)}, \dots, \mathbf{w}_r f^{(r)}$. Let $\mathbf{W} = [\mathbf{w}_1 f^{(1)}, \dots, \mathbf{w}_r f^{(r)}]$ and let the eigenface subspace be generated by the columns of \mathbf{W} . Then the weighted projections of ℓ training face images on the eigenface subspace \mathbf{W} are computed by

$$\mathbf{P}_i = (\mathbf{F}_i - \Psi)\mathbf{W} \in \mathbb{Q}^{m \times r}, \quad i = 1, \dots, \ell, \quad (4.1)$$

where Ψ is the average image of all training samples. Such \mathbf{P}_i is called the *feature matrix* or *feature image* of the sample image \mathbf{F}_i and its j -th column, i.e., $(\mathbf{F}_i - \Psi)\mathbf{w}_j$, is called the *j -th principal component*. In Algorithm 2, we propose the procedure of G2DQPCA with weighted projection for color image recognition.

Algorithm 2 G2DQPCA with Weighted Projection for Color Image Recognition

- 1: For the mean-centered given training samples $\mathbf{F}_i - \Psi$, $i = 1, 2, \dots, \ell$, compute the r ($1 \leq r < n$) projection vectors and their corresponding weighted coefficient by Algorithm 1, denoted by $(\mathbf{w}_1, f^{(1)}), \dots, (\mathbf{w}_r, f^{(r)})$.
 - 2: Let the eigenface subspace be spanned by the columns of $\mathbf{W} = [f^{(1)}\mathbf{w}_1, \dots, f^{(r)}\mathbf{w}_r]$.
 - 3: Compute the projections $\mathbf{P}_1, \dots, \mathbf{P}_r$, defined by (4.1), of ℓ training color images.
 - 4: For a given testing sample \mathbf{F} , compute its feature matrix, $\mathbf{P} = (\mathbf{F} - \Psi)\mathbf{W}$. Seek the nearest face image whose feature matrix $\mathbf{P}_{i^\#}$ ($1 \leq i^\# \leq \ell$) satisfies that $i^\# = \arg \min_{1 \leq i \leq \ell} \|\mathbf{P}_i - \mathbf{P}\|$. Then $\mathbf{F}_{i^\#}$ is output as the person to be recognized.
-

We close this section by applying G2DQPCA to compute the low-rank reconstructions of color images. Let the eigenface subspace be spanned by the columns of $\mathbf{W} = [\mathbf{w}_1, \dots, \mathbf{w}_r]$, where \mathbf{w}_j is computed by Algorithm 1. Then the reconstructions of training samples are computed by

$$\mathbf{F}_i^{rec} = (\mathbf{F}_i - \Psi)\mathbf{W}\mathbf{W}^* + \Psi, \quad i = 1, \dots, \ell. \quad (4.2)$$

That is, we only use the first r projection vectors to reconstruct the original image. One important thing to note here is that the reconstruction process does not need to magnify the effect of features, so the projection matrix \mathbf{W} is unweighted.

One can see that $\mathbf{F}_i^{rec} - \Psi$ is of low-rank since the rank \mathbf{W} is r and r is always a small integer. In fact, we have present a new method to simultaneously compute the low-rank approximations to $\mathbf{F}_i - \Psi$, $i = 1, \dots, \ell$. The reconstruction of testing samples can be computed in the similar way. The whole process is proposed in Algorithm 3.

Algorithm 3 G2DQPCA for Image Reconstruction

- 1: For the mean-centered given training samples $\mathbf{F}_i - \Psi$, $i = 1, 2, \dots, \ell$, compute the r ($1 \leq r < n$) projection vectors by Algorithm 1, denoted by $\mathbf{w}_1, \mathbf{w}_2, \dots, \mathbf{w}_r$.
 - 2: Let the eigenface subspace be spanned by the columns of $\mathbf{W} = [\mathbf{w}_1, \dots, \mathbf{w}_r]$.
 - 3: Compute the reconstructions $\mathbf{F}_1^{rec}, \dots, \mathbf{F}_r^{rec}$ of training samples by (4.2).
 - 4: For a given testing sample \mathbf{F} , compute its reconstruction by $\mathbf{F}^{rec} = (\mathbf{F} - \Psi)\mathbf{W}\mathbf{W}^* + \Psi$.
-

5 EXPERIMENTS

In this section, we evaluate the proposed G2DQPCA and WG2DQPCA models on color face recognition, test the efficiency of G2DQPCA on color image reconstruction and compare WG2DQPCA with four well-known deep learning methods.

The evaluation and comparison are implemented on three standard face databases:

- GTFD—The Georgia Tech Face Database* contains 750 images from 50 subjects, fifth images per subject. All the images are manually cropped, and then resized to 44×33 pixels.
- Color FERET—The color FERET database† contains 1199 persons, 14126 color face images, and each person has various numbers of face images with various backgrounds. The size of each cropped color face image is 192×128 pixels. Here we take 275 individuals and 11 images of each person for testing.
- Faces95—Faces95 database‡ contains 1440 images photographed over a uniform background from 72 subjects, 20 images per subject. The size of each color face image is 200×180 pixels.

Some samples are listed in Figure 3.

Notice that the performance of 2DQPCA has been indicated to be better than 2DPFA in [1], [2] and that 2DQPCA proposed in [1]–[3] are special cases of G2DQPCA with $s = p = 2$. It is only necessary to concentrate on the comparison of G2DQPCA-based approaches with different choices of s and p and the efficiency of utilizing the weighting technique. All numerical experiments are performed with MATLAB-R2016 on a personal computer with Intel(R) Xeon(R) CPU E5-2630 v3 @ 2.4GHz (dual processor) and RAM 32GB.

*. The Georgia Tech face database: http://www.anejian.com/research/face_reco.htm.

†. The color FERET database: <https://www.nist.gov/itl/iad/image-group/color-feret-database>.

‡. The Faces95 database: <https://cswwww.essex.ac.uk/mv/allfaces/faces95.html>.



Fig. 3: Some samples with or without occlusion of one person from the GTFD, Color FERET and Faces95 databases.

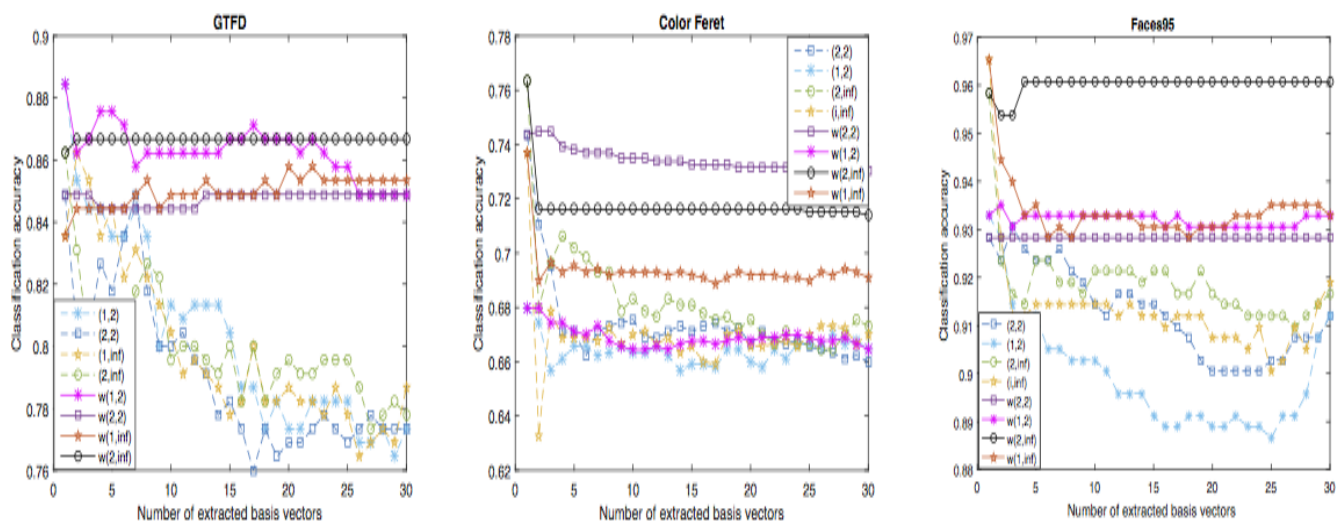


Fig. 4: Classification accuracies of G2DQPCA and WG2DQPCA on the GTFD, Color FERET and Faces95 databases.

Example 5.1 (Color face recognition). In this example, we proceed to investigate the classification performance of G2DQPCA and WG2DQPCA on all three databases with clean training data. Randomly select 90 percent of data set as training set and the remaining as the testing set. The training set is guaranteed to contain at least one image of each individual.

The whole procedure is repeated three times and the average recognition rate is reported. For simplicity, let (s, p) denote G2DQPCA with L_s -norm and L_p -norm, and $w(s, p)$ WG2DQPCA with L_s -norm and L_p -norm in all figures. For instance, $(2, 2)$ represents G2DQPCA with $s = p = 2$, which is exactly the version of 2DQPCA proposed in [1]–[3]; $(1, 2)$, $(1, \text{inf})$ and $(2, \text{inf})$ denote other new versions of 2DQPCA, which are gathered in G2DQPCA. Note that inf means L_∞ -norm. In Figure 4, we present the classification accuracies of G2DQPCA and WG2DQPCA methods applied on three face databases with the number of features increases from 1 to 30.

From the numerical results, one can see that the classification accuracies of WG2DQPCA are much higher than those

of G2DQPCA. The recognition rate of G2DQPCA decreases as the number of features increases, but the recognition rate of WG2DQPCA remains unchanged or perturbs tightly. The optimal parameter pair (s, p) replies on the databases. For the GTFD, Color FERET, and Faces95 databases, the optimal recognition rates are reached when $w(s = 1, p = 2)$, $w(s = 2, p = 2)$ and $w(s = 2, p = \infty)$, respectively. This performance verifies that the G2DQPCA-based approaches with different L_p norms extract quite distant features of color images.

Moreover, 2DQPCA proposed in [1]–[3], indicated by $(2, 2)$ in Figure 4, performs not better than G2DQPCA with $s = 2, p = \infty$ indicated by $(2, \text{inf})$ in most of cases. The classification accuracy of such 2DQPCA is also greatly less than its weighted version, indicated by $w(2, 2)$. That indicates that the proposed weighted G2DQPCA algorithm performs much better than the state-of-the-art 2DQPCA-based approaches in color face recognition.

Example 5.2 (Color face recognition with noisy training data).

In this example, we examine the recognition performance of G2DQPCA and WG2DQPCA with the training set polluted by different kinds and levels of noise, while the testing set are clean. On the three databases, two different noises are considered separately. In the first case, the noise consists of random black and white dots. We randomly added this noise to 20% of the training set. The location of noise is arbitrary, and the size is at least 10×10 . The second case is to add salt and pepper noise to the training set. Here we set the noise density as 0.02, 0.05 and 0.1, respectively.

The whole procedure of each case is repeated three times and the average result is reported. In Figures 5, 6 and 7, we present the average classification accuracy of compared methods when the training set is polluted by different kinds and levels of noises:

(a) The training set is polluted by black and white dots noises.

(b)-(d) The training set is polluted by salt and pepper noises and the noise densities are 0.02, 0.05 and 0.1, respectively.

The numerical results indicate that the pollution on the training set impacts the classification performance since the feature extraction is perturbed by noise.

It is still true that the recognition rate of WG2DQPCA is more stable and higher than that of G2DQPCA. Obviously, under the influence of different noises, the optimal parameter pair $w(s, p)$ is not fixed for all databases. In Figure 5, it is shown that for GTFD database, WG2DQPCA with $s = 2$ and $p = 2$ has good performance in the case of black and white dots noise; WG2DQPCA with $s = 1$ and $p = \infty$ works well when the salt and pepper noise density are 0.02 and 0.05; and WG2DQPCA with $s = 1$ and $p = 2$ performs better in the last case. For Faces95 database, the numerical results in Figure 6 indicate that WG2DQPCA with $s = 2$ and $p = \infty$ achieves the highest classification accuracy in all cases. As for Color FERET database, it is observed that the performance of WG2DQPCA with $s = 2$ and $p = 2$ is relatively stable from Figure 7. It can be concluded that the weighing technique not only promotes the performance of G2DQPCA, but also helps G2DQPCA to resist the pollution of noises.

Example 5.3 (Color image reconstruction). In this example, we evaluate the reconstruction performance of G2DQPCA algorithm. Here 20% of the three databases have randomly selected to add black and white dots noise, respectively.

The following reconstruction error is used to measure the quality of methods:

$$err = \frac{1}{\ell} \sum_{i=1}^{\ell} \|\mathbf{F}_i^{\text{clean}}(\mathbf{I} - \mathbf{W}\mathbf{W}^*)\|_F \quad (5.1)$$

where ℓ is the number of clean training data, $\mathbf{F}_i^{\text{clean}}$ is the i -th clean training sample and \mathbf{W} is the projection matrix trained on the whole polluted training database. As emphasized in Section 4, \mathbf{W} is unweighted because the process of reconstruction does not need to magnify the effect of features.

In the first graph of Figure 8, we show the reconstruction errors of G2DQPCA in several special cases with the number of features from 1 to 20 on GTFD database. In the second and third graphs of Figure 8, we present the reconstruction errors of G2DQPCA with the feature number from 1 to 30 on the other two databases. From the numerical results, all parameter pairs are indicated to have a good performance in image reconstruction. With the increase of features number, it is observed that applying L_1 -norm on the objective function, i.e., $s = 1, p = 2$, is

effective for the images reconstruction on GTFD database and Color FERET database. G2DQPCA works well on the Faces95 database when $s = 2, p = 2$ and $s = 2, p = \infty$.

As an illustration, several reconstructed images are listed in Figures 9, 10 and 11. The first column are the images to be reconstructed. The following three columns are the reconstructed images by using the first 20 projection vectors of G2DQPCA wherein the (s, p) pairs are set to be $(1, 2)$, $(2, 2)$ and $(2, 1)$ in order. The last column shows the original images for comparison.

Example 5.4 (Comparison with deep learning methods). In this experiment, we compare WG2DQPCA with four prominent deep learning primitives: Convolutional Neural Networks (CNNs), Deep Neural Networks (DNNs), Deep Belief Networks (DBNs) and Recurrent Neural Networks (RNNs).

- DNNs are implemented by stacking layers of neural networks along the depth and width of smaller architectures. For GTFD and Faces95 databases, we increase the number of hidden neurons in first DNN from 8 to 588, step 20, and the number of neurons in second and third hidden layers are set as 512 and 512. For Color FERET database, we increase the number of hidden neurons in first DNN from 208 to 788 with step 20, and the number of neurons in second and third hidden layers are set as 512 and 512.
- CNNs are feed-forward, back-propagate neural networks with a special architecture inspired from the visual system, consisting of alternating layers of convolution layers and sub-sampling layers. In our experiments, we set a convolution layer and a sub-sampling layer. The convolution layer has k feature maps, where we increase k from 8 to 588 with step 20, connected to the single input layer through $k \ 5 \times 5$ kernels.
- DBNs consist of a number of layers of Restricted Boltzmann Machines (RBMs) which are trained in a greedy layer wise fashion. We increase the number of hidden neurons in first RBM from 8 to 588 with step 20 and set a fixed number of hidden neurons of 256 in second RBM.
- RNNs is a kind of recurrent neural networks which takes sequence data as input, recurses in the evolution direction of sequence, and all nodes are connected in chain. We increase the number of hidden neurons from 8 to 588 with step 20.

The comparison is implemented on color face recognition with using the GTFD, Color FERET, and Faces95 databases. We randomly select 90 percent of data set as the training set and the remaining as the testing set.

From Example 5.1, it has been observed that WG2DQPCA obtains optimal recognition rates on the GTFD, Color FERET, and Faces95 databases when $w(s = 1, p = 2)$, $w(s = 2, p = 2)$ and $w(s = 2, p = \infty)$, respectively. So we fix these optimal values of s and p for WG2DQPCA during the comparison.

In the test process, we found that if the number of iterations (epoch) is small, the recognition rates of neural networks are low. With increasing iteration times, their recognition rates will increase, but they are easy to overfit. Overfitting means that the model has a small error on the training set but a large error on the test set. Take the GTFD database as an example. The numerical results are shown in Figure 12. The lines ' - o - ' and ' - * - ' represent the classification accuracies of training

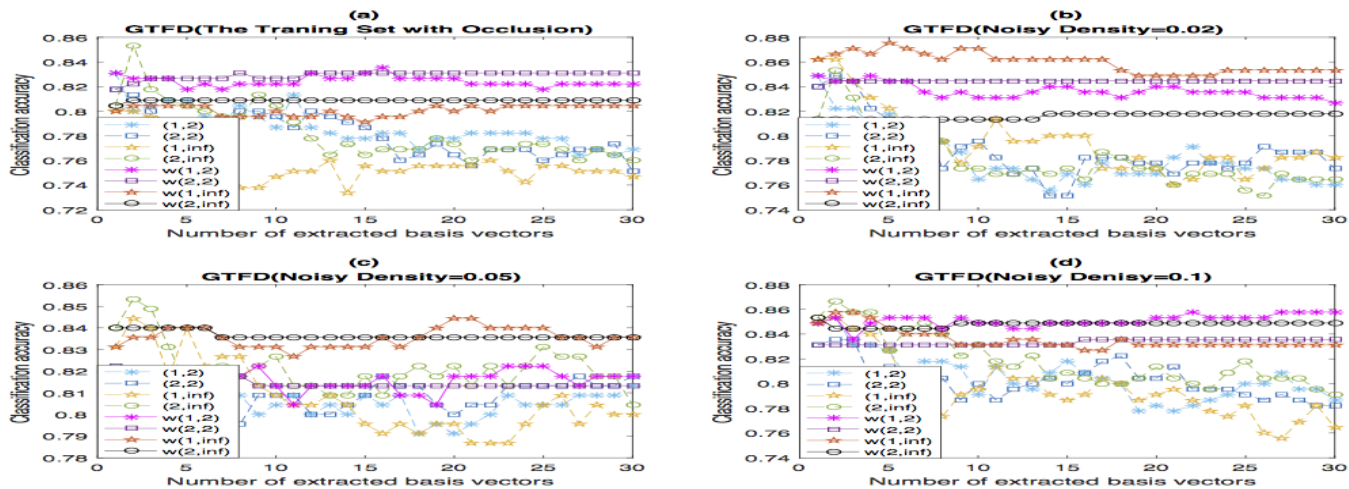


Fig. 5: Classification accuracies with polluted training set of G2DQPCA and WG2DQPCA on the GTFD database.

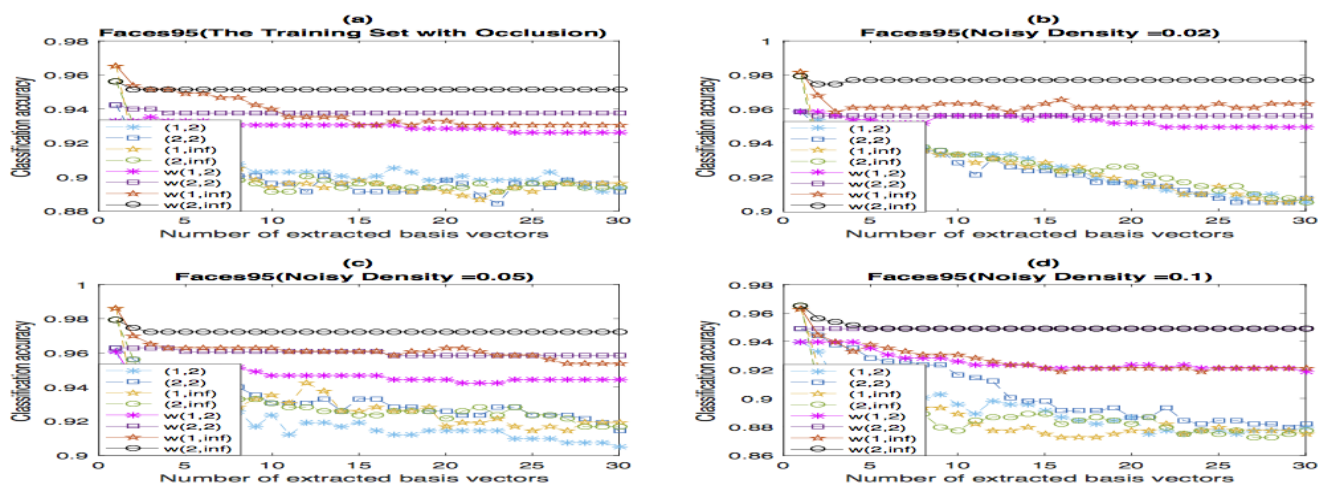


Fig. 6: Classification accuracies with polluted training set of G2DQPCA and WG2DQPCA on the Faces95 database.

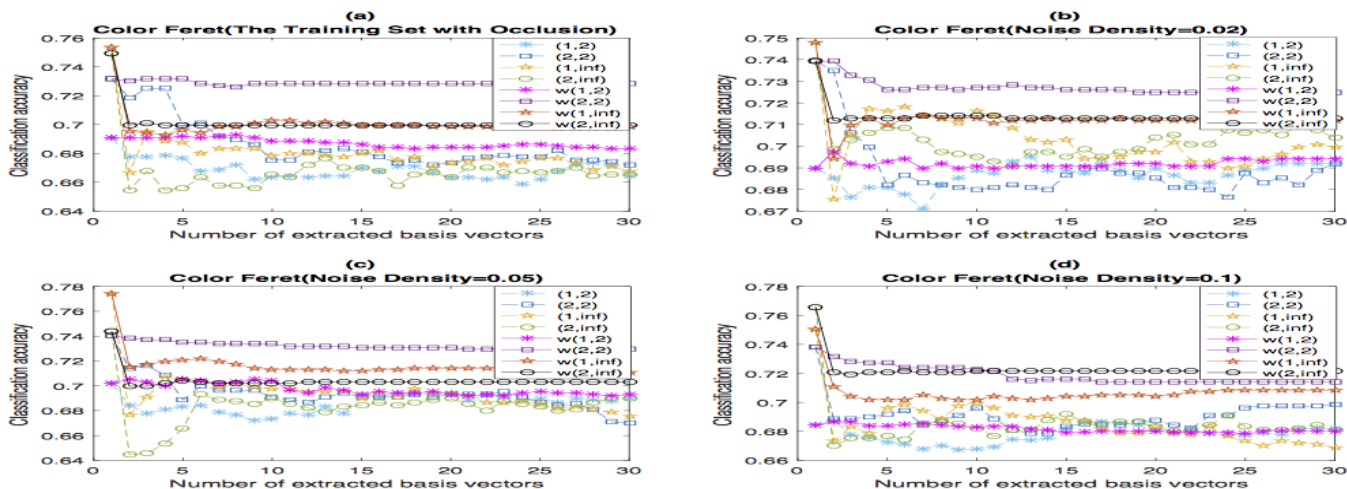


Fig. 7: Classification accuracies with polluted training set of G2DQPCA and WG2DQPCA on the Color FERET database.

and testing samples, respectively. The fuchsia, black, red and blue lines represent the classification accuracies with epoch=1, 5, 10, 15. From Figure 12, we can see that the neural networks have high accuracy but have only slight overfitting phenomenon when the

epochs of DNNs, CNNs and RNNs are respectively 10, 5 and 10, respectively. After that, the overfitting happens, i.e., the 'o' line becomes higher than the '*' line. The recognition rates of DBNs are always low. So in this experiment, set epoch=10 for

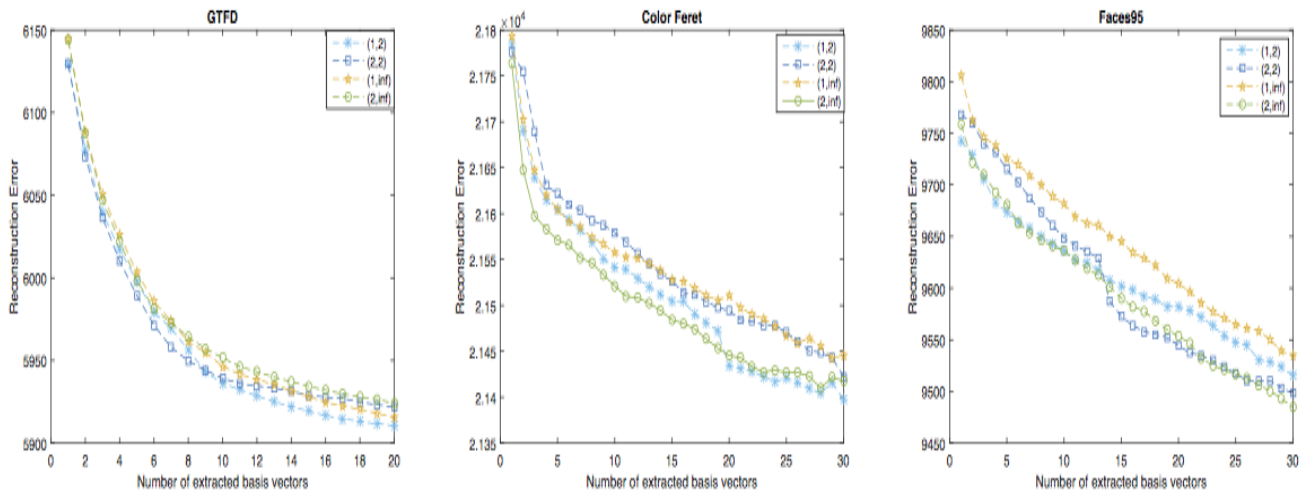


Fig. 8: Reconstruction errors of G2DQPCA on the GTFD, Color FERET and Faces95 databases.



Fig. 9: The reconstructed images by G2DQPCA on two sample images from the polluted GTFD database.

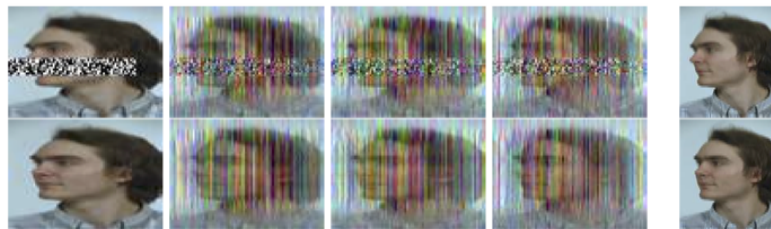


Fig. 10: The reconstructed images by G2DQPCA on two sample images from the polluted Color FERET database.



Fig. 11: The reconstructed images by G2DQPCA on two sample images from the polluted Faces95 database.

DNNs, DBNs and RNNs, and epoch=5 for CNNs. It should be noticed that the recognition rates of CNNs, DNNs, DBNs and RNNs can not achieve at high levels with small samples.

The numerical results are shown in Figure 13. The average recognition rates of WG2DQPCA, CNNs, DNNs, DBNs and RNNs are 0.89, 0.67, 0.54, 0.01 and 0.37, respectively; and the maximum recognition rates are 0.9, 0.77, 0.71, 0.03 and 0.59. It

indicates that WG2DQPCA performs better than CNNs, DNNs, DBNs and RNNs on color face recognition.

The above performance of G2DQPCA and WG2DQPCA can be understood by the following analysis. G2DQPCA is in fact to extract a number of principal components (features) of all color images in the training set, which can

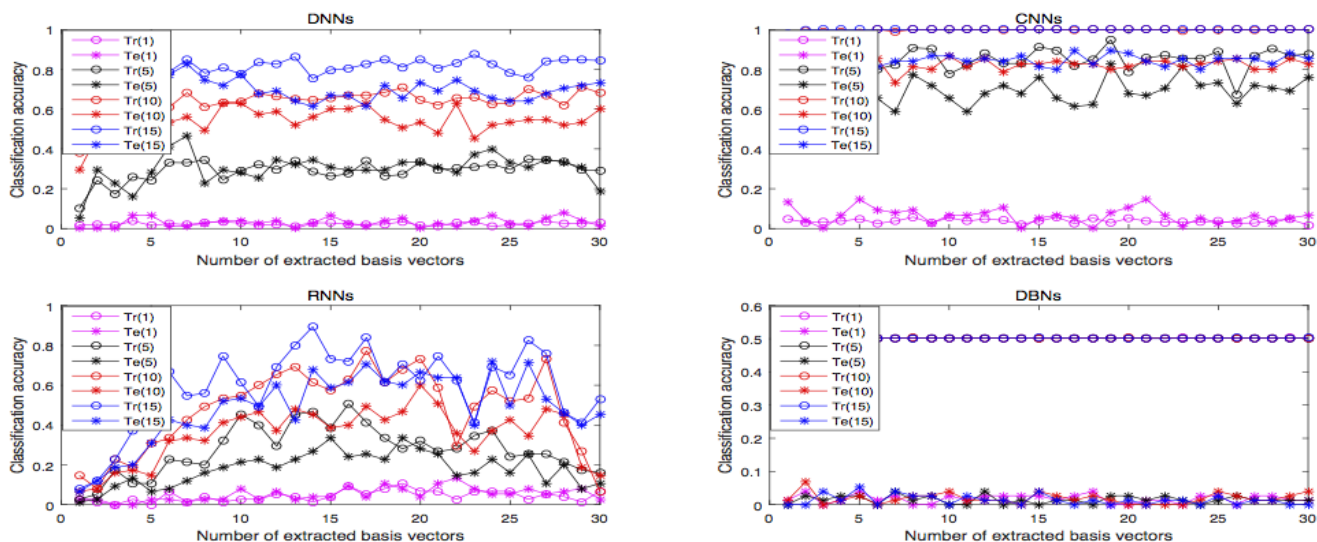


Fig. 12: Classification accuracies with different epoch of CNNs, DNNs, DBNs and RNNs on the GTFD database.

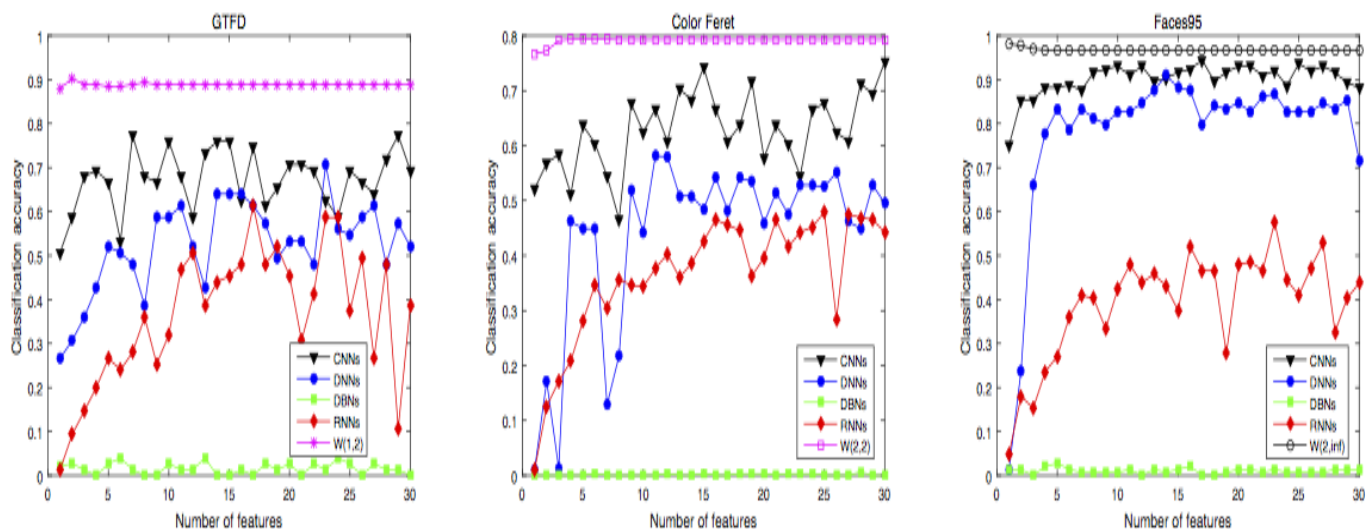


Fig. 13: Classification accuracies of WG2DQPCA, CNNs, DNNs, DBNs and RNNs on the GTFD, Color FERET and Faces95 databases.

be used to reconstruct the optimal low-rank approximations of original color images. The projections under the exacted features has the largest variance measured by the L_p norm in the objective function. The proposed weighting technique enhances the role of principal components and thus WG2DQPCA performs better than G2DQPCA in color image recognition. Generally, the noise influence often exists in the high frequency components, but not in the principal (low frequency) components. That is why the reconstruction has the efficiency of noise reduction.

6 CONCLUSION

In order to extract more types of geometric features of color images, this paper proposes a generalized two-dimensional quaternion principal component analysis method and a color image recognition model based on this method. The quaternion optimization problem in the model is equivalently transformed into a real optimization problem and

a fast algorithm is proposed as well as the convergence analysis theory. The proposed principle component weighting strategy helps overcome the odd phenomenon that the recognition rate of the color image recognition model based on the traditional two-dimensional quaternion principal component analysis method decreases with the increase of principal components. Numerical experiments indicate that the proposed method has a higher face recognition rate than the state-of-the-art methods of the same type and four well-known deep learning methods in color image recognition. Even so, our method still has several aspects to be improved. For instance, there is no theory to determine the optimal values of model parameters. A possible solution is to use the validation set for data-driven parameter selection.

REFERENCES

- [1] Z. Jia, S. Ling and M. Zhao, *Color two-dimensional principal component analysis for face recognition based on quaternion model*, LNCS, 10361

- (2017) 177-189.
- [2] M. Zhao, Z.G. Jia and D. Gong, *Improved Two-Dimensional Quaternion Principal Component Analysis*, IEEE Access, 7 (2019) 79409-79417.
 - [3] X. Xiao and Y. Zhou, *Two-Dimensional Quaternion PCA and Sparse PCA*, IEEE Trans. Neur. Net. Lear., 30(7) (2019) 2028-2042.
 - [4] X. Xiao, Y. Chen, Y. Gong and Y. Zhou, *2D Quaternion Sparse Discriminant Analysis*, IEEE Trans. Image Process., 29(1) (2020) 2271-2286.
 - [5] M. Zhao, Z. Jia, Y. Cai, X. Chen and D. Gong *Advanced Variations of two-dimensional principal component analysis for face recognition*, Neurocomputing, 452(2021), 653-664.
 - [6] J. Yang, D. Zhang, A. F. Frangi, and J. Y. Yang, *Two-dimensional PCA: A new approach to appearance-based face representation and recognition*, IEEE Trans. Pattern Anal. Mach. Intell., 26(1) (2004) 131-137.
 - [7] M. A. Turk and A. P. Pentland, *Face recognition using eigenfaces*, Proc. IEEE Conf. Comput. Vis. Pattern Recognit., (1991) 586-591.
 - [8] Q. Ke and T. Kanade, *Robust L_1 norm factorization in the presence of outliers and missing data by alternative convex programming*, IEEE Conf. Comput. Vis. Pattern Recognit., San Diego, CA, USA, 2005, 739-746.
 - [9] C. Ding, D. Zhou, X. He, and H. Zha, *R_1 -PCA: Rotational invariant L_1 -norm principal component analysis for robust subspace factorization*, Proc. Int. Conf. Machine Learning (ICML 2006), (2006) 281-288.
 - [10] N. Kwak, *Principal component analysis based on L_1 -norm maximization*, IEEE Trans. Pattern Anal. Mach. Intell., 30 (9) (2008) 1672-1680.
 - [11] S. Boyd and L. Vandenberghe, *Convex Optimization*, Cambridge university press, 2009.
 - [12] H. Zou and T. Hastie, *Regularization and variable selection via the elastic net*, Journal of the Royal Statistical Society: Series B (Statistical Methodology), 67(2) (2005) 301-320.
 - [13] H. Zou, T. Hastie and R. Tibshirani, *Sparse principal component analysis*, J. Comput. Graph. Stat., 15(2) (2006) 265-286.
 - [14] H. Shen and J. Z. Huang, *Sparse principal component analysis via regularized low rank matrix approximation*, J. Multivar. Anal., 99(6) (2008) 1015-1034.
 - [15] M. Journée, Y. Nesterov, P. Richtárik, and R. Sepulchre, *Generalized power method for sparse principal component analysis*, J. Mach. Learn. Res., 11 (2010) 517-553.
 - [16] F. R. On, R. Jailani, S. L. Hassan and N. M. Tahir, *Analysis of sparse PCA using high dimensional data*, 2016 IEEE 12th International Colloquium on Signal Processing & Its Applications (CSPA2016), (2016) 340-345.
 - [17] M. I. Razzak, R. A. Saris, M. Blumenstein and G. Xu, *Robust 2D Joint Sparse Principal Component Analysis With F-Norm Minimization For Sparse Modelling: 2D-R/SPCA*, International Joint Conference on Neural Networks (IJCNN), (2018) 1-7.
 - [18] D. Meng, Q. Zhao, and Z. Xu, *Improve robustness of sparse PCA by L_1 -norm maximization*, Pattern Recognit., 45 (1) (2012) 487-497.
 - [19] P. Peng, Y. Zhang, F. Liu, H. Wang and H. Zhang, *A Robust and Sparse Process Fault Detection Method Based on RSPCA*, IEEE Access, 7 (2019) 133799-133811.
 - [20] Z. Liang, S. Xia, Y. Zhou, L. Zhang, and Y. Li, *Feature extraction based on L_p -norm generalized principal component analysis*, Pattern Recognit. Lett., 34(9) (2013) 1037-1045.
 - [21] N. Kwak, *Principal component analysis by L_p -norm maximization*, IEEE Trans. Cybern., 44(5) (2014) 594-609.
 - [22] J. Ye, *Generalized low rank approximations of matrices*, Mach. Learn., 61 (2005) 167-191.
 - [23] D. Zhang and Z.-H. Zhou, *$(2D)^2$ PCA: Two-directional twodimensional PCA for efficient face representation and recognition*, Neurocomputing, 69(1) (2005) 224-231.
 - [24] X. Li, Y. Pang, and Y. Yuan, *L_1 -norm-based 2DPCA*, IEEE Trans. Syst., Man, Cybern. B, Cybern., 40 (4) (2010) 1170-1175.
 - [25] J. Meng and X. Zheng, *Robust sparse 2DPCA and its application to face recognition*, Symposium on Photonics and Optoelectronics, (2012) 1-4.
 - [26] J. Wang, *Generalized 2-D Principal Component Analysis by L_p -Norm for Image Analysis*, IEEE Trans. Cybern., 46(3) (2016) 792-803.
 - [27] X. Chen, Z.-G. Jia, Y.-F. Cai and M.-X. Zhao, *Relaxed 2-D principal component analysis by L_p norm for face recognition*, arXiv e-prints, (2019) arXiv:1905.06458.
 - [28] J. Mairal, M. Elad, and G. Sapiro, *Sparse representation for color image restoration*, IEEE Trans. Image Process., 17(1) (2008) 53-69.
 - [29] R. Lan and Y. Zhou, *Quaternion-michelson descriptor for color image classification*, IEEE Trans. Image Process., 25(11) (2016) 5281-5292.
 - [30] X. Xiang, J. Yang, and Q. Chen, *Color face recognition by PCA-like approach*, Neurocomputing, 152 (2015) 231-235.
 - [31] C. Zou, K. I. Kou and Y. Wang, *Quaternion Collaborative and Sparse Representation With Application to Color Face Recognition*, IEEE Trans. Image Process. 25(7) (2016) 3287-3302.
 - [32] N. L. Bihan and S. J. Sangwine, *Quaternion principal component analysis of color images*, Proc. 2003 Tenth IEEE Int. Conf. Image Processing (ICIP 2003), 1 (2003) 809-812.
 - [33] Y. F. Sun, S. Y. Chen and B. C. Yin, *Color face recognition based on quaternion matrix representation*, Pattern Recognit. Lett., 32(4)(2011) 597-605.
 - [34] B. J. Chen, J. H. Yang, B. Jeon and X. P. Zhang, *Kernel quaternion principal component analysis and its application in RGB-D object recognition*, Neurocomputing, 266(29) (2017) 293-303.
 - [35] J. Ye and Q. Li, *A two-stage linear discriminant analysis via QR decomposition*, IEEE Trans. Pattern Anal. Mach. Intell., 27(6) (2005) 929-941.
 - [36] S. Noushath, G. Hemantha Kumar and P. Shivakumara, *$(2D)^2$ LDA: An efficient approach for face recognition*, Pattern Recognit., 39(7) (2006) 1396-1400.
 - [37] Z. Liang, Y. Li and P. Shi, *A note on two-dimensional linear discriminant analysis*, Pattern Recognit. Lett., 29(16) (2008) 2122-2128.
 - [38] Z. Jia, M. K. Ng and G. Song, *Lanczos method for large-scale quaternion singular value decomposition*, Numer. Algor. 82(2) (2019) 699-717.
 - [39] Z. Jia, M. K. Ng and G. Song, *Robust quaternion matrix completion with applications to image inpainting*, Numer. Linear Algebra Appl., 26(4) (2019) e2245.
 - [40] Z. Jia, M. K. Ng and W. Wang, *Color image restoration by saturation-value total variation*, SIAM J. Imaging Sci., 12(2) (2019) 972-1000.
 - [41] Y. Chen, X. Xiao and Y. Zhou, *Low-Rank Quaternion Approximation for Color Image Processing*, IEEE Trans. Image Process. 29(1) (2020) 1426-1439.
 - [42] D. R. Hunter and K. Lange, *A tutorial on MM algorithms*, The American Statistician, 58(1) (2004) 30-37.
 - [43] S. C. Pei and C. M. Cheng, *Quaternion matrix singular value decomposition and its applications for color image processing*, Proc. 2003 Int. Conf. Image Processing (ICIP 2003), 1 (2003) 805-808.
 - [44] Z. Jia, M. Wei, S. Ling, *A new structure-preserving method for quaternion Hermitian eigenvalue problems*, J. Comput. Appl. Math. 239(2013) 12-24.
 - [45] Z. Jia, M. Wei, M. Zhao and Y. Chen, *A New Real Structure-preserving Quaternion QR Algorithm*, J. Comput. Appl. Math., 343 (2018) 26-48.
 - [46] W. H. Yang, *On generalized Hölder inequality*, Nonlinear Analysis: Theory, Methods & Applications, 16(5) (1991) 489-498 .
 - [47] S. Boyd and L. Vandenberghe. *Convex Optimization*. Cambridge University Press, 2004 : 727.

7 APPENDIX

To be self-contained, we present some important results in this appendix.

7.1 Properties of convex and concave functions

The following theorem explains the property of convex functions [47].

THEOREM 7.1. *Let S be a non-empty open convex set in \mathbb{R}^n , and let f be a function with a first-order continuous derivative function, i.e., $f \in C^1(S)$. Then f is a convex function if and only if for all $w, v \in S$,*

$$f(w) \geq f(v) + \nabla f(v)^T(w - v). \quad (7.1)$$

Proof. Let f be a convex function. In other words, for all $w, v \in S, \lambda \in (0, 1)$,

$$f(\lambda w + (1 - \lambda)v) \leq \lambda f(w) + (1 - \lambda)f(v). \quad (7.2)$$

Meanwhile,

$$\begin{aligned} f(\lambda w + (1 - \lambda)v) &= f(v + \lambda(w - v)) \\ &= f(v) + \lambda \nabla f(v)^T(w - v) \\ &\quad + O(\lambda \|w - v\|), \end{aligned}$$

where $O(\lambda \|w - v\|) \rightarrow 0$ when $\|w - v\| \rightarrow 0$.

Dividing by λ on both sides, we get

$$f(w) \geq f(v) + \nabla f(v)^T(w - v).$$

Conversely, since S is convex, then for all $w, v \in S, \lambda \in (0, 1)$, let $z = \lambda w + (1 - \lambda)v \in S$. By the condition (7.1), we have that

$$f(w) \geq f(z) + \nabla f(z)^T(w - z), \quad (7.3a)$$

$$f(v) \geq f(z) + \nabla f(z)^T(v - z). \quad (7.3b)$$

Thus, combining the above equations, we get

$$\begin{aligned} \lambda f(w) + (1 - \lambda)f(v) &\geq \lambda f(z) + \lambda \nabla f(z)^T(w - z) \\ &\quad + (1 - \lambda)f(z) + (1 - \lambda) \nabla f(z)^T(v - z) \\ &= f(z) + \nabla f(z)^T(\lambda w + (1 - \lambda)v - z) \\ &= f(\lambda w + (1 - \lambda)v). \end{aligned}$$

Therefore, f is a convex function. \square

Next, we consider concave functions.

THEOREM 7.2. *Let S be a non-empty open convex set in \mathbb{R}^n , $f \in C^1(S)$. Then f is a concave function if and only if for all $w, v \in S$,*

$$f(w) \leq f(v) + \nabla f(v)^T(w - v). \quad (7.4)$$

Proof. The proof of Theorem 7.2 is similar to that of Theorem 7.1. The only difference is that we need to replace the " \geq " with " \leq " in (7.2) as well as in other formulas. \square

7.2 Proof of equation (3.5)

By the definition, we can get

$$\begin{aligned} |\mathbf{v}^{(\gamma)}|_Q^{p-1} &= (|\mathbf{v}|^{p-1} + |\mathbf{v}|^{p-1}\mathbf{i} + |\mathbf{v}|^{p-1}\mathbf{j} + |\mathbf{v}|^{p-1}\mathbf{k})^{(\gamma)} \\ &= [(|\mathbf{v}|^{p-1})^T (|\mathbf{v}|^{p-1})^T (|\mathbf{v}|^{p-1})^T (|\mathbf{v}|^{p-1})^T]^T, \end{aligned}$$

and

$$\begin{aligned} \text{signQ}(\mathbf{v}^{(\gamma)}) &= (\text{sign}(\mathbf{v}))^{(\gamma)} \\ &= \left[\left[\frac{v_i^{(0)}}{|\mathbf{v}_i|} \right]_n^T \left[\frac{v_i^{(1)}}{|\mathbf{v}_i|} \right]_n^T \left[\frac{v_i^{(2)}}{|\mathbf{v}_i|} \right]_n^T \left[\frac{v_i^{(3)}}{|\mathbf{v}_i|} \right]_n^T \right]^T. \end{aligned}$$

Thus, we have

$$\begin{aligned} &|\mathbf{v}^{(\gamma)}|_Q^{p-1} \circ \text{signQ}(\mathbf{v}^{(\gamma)}) \\ &= \left[\left[|\mathbf{v}_i|^{p-2} v_i^{(0)} \right]_n^T \left[|\mathbf{v}_i|^{p-2} v_i^{(1)} \right]_n^T \left[|\mathbf{v}_i|^{p-2} v_i^{(2)} \right]_n^T \left[|\mathbf{v}_i|^{p-2} v_i^{(3)} \right]_n^T \right]^T. \end{aligned} \quad (7.5)$$

Above all, it naturally derives that

$$\begin{aligned} &(|\mathbf{v}^{(\gamma)}|_Q^{p-1} \circ \text{signQ}(\mathbf{v}^{(\gamma)}))^T \mathbf{v}^{(\gamma)} \\ &= \sum_{i=1}^n |\mathbf{v}_i|^{p-2} [(v_i^{(0)})^2 + (v_i^{(1)})^2 + (v_i^{(2)})^2 + (v_i^{(3)})^2] \\ &= \sum_{i=1}^n |\mathbf{v}_i|^{p-2} |\mathbf{v}_i|^2 = \sum_{i=1}^n |\mathbf{v}_i|^p = \|\mathbf{v}^{(\gamma)}\|_{2,p}^p. \end{aligned}$$

7.3 Proof of equation (3.22)

From equation (3.21), it's not difficult to understand that

$$(\mathbf{u}^{(\gamma)})^{(k)} = |(\mathbf{v}^{(\gamma)})^{(k)}|_Q^{q-1} \circ \text{signQ}((\mathbf{v}^{(\gamma)})^{(k)}).$$

Then, we give an explanation

$$\|(\mathbf{v}^{(\gamma)})^{(k)}\|_{2,q}^{q-1} = \|(\mathbf{u}^{(\gamma)})^{(k)}\|_{2,p}.$$

By the equation (7.5),

$$\begin{aligned} \|\mathbf{u}^{(\gamma)}\|_{2,p} &= \| |(\mathbf{v}^{(\gamma)})^{(k)}|_Q^{q-1} \circ \text{signQ}(\mathbf{v}^{(\gamma)}) \|_{2,p} \\ &= \| |(\mathbf{v}^{(\gamma)})^{(k)}|_Q^{q-1} \|_{2,p}. \end{aligned}$$

Recalling the definition of $L_{2,p'}$ -norm, we obtain

$$\|(\mathbf{u}^{(\gamma)})^{(k)}\|_{2,p} = \left[\sum_{i=1}^n (|(v_i^{(\gamma)})^{(k)}|_Q^{q-1})^p \right]^{\frac{1}{p}}.$$

Let $\frac{1}{p} + \frac{1}{q} = 1$, then

$$\begin{aligned} \|\mathbf{u}^{(\gamma)}\|_{2,p} &= \left[\sum_{i=1}^n |(v_i^{(\gamma)})^{(k)}|_Q^{q-1} \right]^{\frac{q-1}{q}} \\ &= \left[\left(\sum_{i=1}^n |(v_i^{(\gamma)})^{(k)}|_Q \right)^{\frac{1}{q}} \right]^{q-1} \\ &= \|(\mathbf{v}^{(\gamma)})^{(k)}\|_{2,q}^{q-1}. \end{aligned}$$

7.4 Proof of equation (3.29)

Now we consider the partial derivative with respect to $\mathbf{w}^{(\gamma)}$:

$$\left[\frac{\partial h(\mathbf{w}^{(\gamma)})}{\partial \mathbf{w}^{(\gamma)}} \right]_l = \frac{\partial h(\mathbf{w}^{(\gamma)})}{\partial w_i^{(j)}}.$$

Considering the partial derivative

$$\left[\frac{\partial |\mathbf{w}|}{\partial w_i^{(j)}} \right]_l = \frac{\partial}{\partial w_i^{(j)}} |\mathbf{w}_i| = \frac{w_i^{(j)}}{|\mathbf{w}_i|}.$$

Then

$$\left[\frac{\partial h(\mathbf{w}^{(\gamma)})}{\partial \mathbf{w}^{(\gamma)}} \right]_l = s(\mathbf{v}^{(k)})_i^{(j)} - \lambda p \left[|\mathbf{w}_i^{(k)}|^{p-1} \frac{w_i^{(j)}}{|\mathbf{w}_i|} \right].$$